EFDA–JET–PR(13)24

J.R.Martin-Solis, A. Loarte, E.M. Hollmann, B. Esposito, V. Riccardo,
FTU and DIII-D Teams and JET EFDA contributors

# Inter-Machine Comparison of the Termination Phase and Energy Conversion in Tokamak Disruptions with Runaway Current Plateau Formation and Implications for ITER

# Inter-Machine Comparison of the Termination Phase and Energy Conversion in Tokamak Disruptions with Runaway Current Plateau Formation and Implications for ITER

J.R.Martin-Solis[1], A. Loarte[2], E.M. Hollmann[3], B. Esposito[4], V. Riccardo[5], FTU[4] and DIII-D[3] Teams, and and JET EFDA contributors*

***JET-EFDA, Culham Science Centre, OX14 3DB, Abingdon, UK***

*[1]Universidad Carlos III de Madrid, Avenida de la Universidad 30, 28911-Madrid, Spain*
*[2]ITER Organization, Route de Vinon sur Verdon, 13115 St Paul Lez Durance, France*
*[3]University of California-San Diego, La Jolla, California 92093-0417, USA*
*[4]Associazione Euratom-ENEA sulla Fusione, C.R. Frascati, C.P. 65, 00044-Frascati, Roma, Italy*
*[5]EURATOM-CCFE Fusion Association, Culham Science Centre, OX14 3DB, Abingdon, OXON, UK*
** See annex of F. Romanelli et al, "Overview of JET Results", (24th IAEA Fusion Energy Conference, San Diego, USA (2012)).*

Preprint of Paper to be submitted for publication in
Nuclear Fusion

**ABSTRACT.**
The termination of the current and the loss of runaway electrons following runaway current plateau formation during disruptions have been investigated in the JET, DIII-D and FTU tokamaks. Substantial conversion of magnetic energy into runaway kinetic energy, up to ~10 times the initial plateau runaway kinetic energy, has been inferred for the slowest current terminations. Both, modelling and experiment suggest that, in present devices, the efficiency of conversion into runaway kinetic energy is determined to a great extent by the characteristic runaway loss time, $\tau_{diff}$, and the resistive time of the residual ohmic plasma after the disruption, $\tau_{res}$, increasing with the ratio $\tau_{diff}/\tau_{res}$. It is predicted that, in large future devices such as ITER, the generation of runaways by the avalanche mechanism will play an important role, particularly for slow runaway discharge terminations, increasing substantially the amount of energy deposited by the runaways onto the plasma facing components by the conversion of magnetic energy of the runaway plasma into runaway kinetic energy. Estimates of the power fluxes on the beryllium plasma facing components during runaway termination in ITER indicate that for runaway currents of up to 2MA no melting of the components is expected. For larger runaway currents, minimization of the effects of runaway impact on the first wall requires a reduction of the kinetic energy of the runaway beam before termination and, in addition, high plasma density ne and low ohmic plasma resistance (long $\tau_{res}$) to prevent large conversion of magnetic into runaway kinetic energy during slow current terminations.

## 1. INTRODUCTION

The low temperatures following the thermal quench of a tokamak disruption result in a significant increase of the plasma resistivity and, hence, of the electric field which can lead to the generation of large amounts of runaway electrons with energies as high as several tens of MeV during the current quench phase of the disruption [1]. Runaway electron current plateaus of a few mega-amps have indeed been reported in large tokamaks like JET or JT-60U [2, 3], and it is expected that significant runaway currents will be much more likely during "uncontrolled" disruptions in next step devices like ITER [4]. These energetic electrons are found to cause damage (melting or brittle destruction) when they impact on the first wall (FW) plasma facing components [5]. Runaway electrons are usually found to deposit their energy in very short pulses and on localized areas of the plasma facing components which lead to a substantial reduction of their lifetime and, in some cases, even require their replacement after a single event [6].

Figure 1 shows a JET disruption with formation of a runaway current plateau of ~0.9MA with the typical phases of current quench, runaway plasma plateau and runaway plasma termination for a disruption with runaway formation. Most of the experimental and theoretical work on runaways has focused so far on the identification of the mechanisms determining the formation of the runaway population during the current quench of the disruption and on the prediction of the runaway current level and of the runaway kinetic energy expected in ITER [7, 8, 9, 10, 11, 12]. It has been predicted that a substantial fraction of the plasma current, as much as two thirds of the predisruption current,

might be converted into runaway current during an ITER disruption [12, 13], mainly due to the avalanche mechanism, in which runaways kick thermal electrons past the critical energy and convert them into runaways [14, 15]. Although highly relativistic, the total kinetic energy carried by the runaway electrons is much lower than the energy stored in the poloidal magnetic field of the runaway plasma itself. If we assume the runaway current formation to be dominated by avalanche, at high electric field the evolution of the runaway current, Ir, in the disruptive plasma is given by [16],

$$\frac{dI_r}{dt} = \frac{I_r}{\tau_s} \approx \frac{eE_{||}}{m_e\, c\, ln\Lambda\; a(Z_{eff})}, \tag{1}$$

where $\tau_s \approx m_e c \ln\Lambda\, a(Z_{eff})/eE_{||}$ is the the characteristic time for avalanching associated with secondary electron generation, and $a(Z_{eff}) \approx \sqrt{(3 + Z_{eff})/\pi}$ (e is the absolute value of the electron charge, $m_e$ is the electron mass, $E_{||}$ is the toroidal electric field, $Z_{eff}$ is the effective ion charge, and $\ln\Lambda$ is the Coulomb logarithm).

In these conditions, the energy absorbed by the runaway electrons in form of kinetic energy through their acceleration during the disruption can be approximated by

$$W_{run} \approx 2\pi R_0 \int I_r E_{||}\, dt \approx \frac{2\pi R_0\, m_e c\, ln\Lambda\; a(Z_{eff})}{e} I_r \tag{2}$$

($R_0$ is the plasma major radius) which, for typical ITER conditions ($I_r$ ~10MA; $R_0 \approx 6.2$m) yields $W_{run}$ ~20–30MJ.

On the other hand, the ratio of the runaway kinetic energy to the magnetic energy of the runaway plasma ($W_{mag} = L_p I_r^2/2$, where $L_p$ is the plasma inductance) is given by,

$$\frac{W_{run}}{W_{mag}} \sim \frac{4\pi R_0\, m_e c\, ln\Lambda\; a(Z_{eff})}{e\, L_p\, I_r} \sim 2 - 4\% \tag{3}$$

(where the total plasma inductance, $L_p \sim 16\mu$H, has been used) so that the total magnetic energy of the runaway plasma is much larger than its kinetic energy.

Although the main interest of studying runaway plasmas is related to their final deposition on plasma facing components, much less attention has been paid to their termination phase. In this phase, the runaway plateau plasma becomes unstable, and the plasma current and the runaway electrons are lost (see Fig.1). During this runaway termination phase, conversion of the magnetic energy of the runaway plasma into runaway kinetic energy can occur. This can increase substantially the energy fluxes deposited by the runaway electrons on the plasma facing components in comparison with the values expected from the runaway kinetic energy gain during the initial current quench of the disruption [Eq.(2)]. Despite the obvious importance of this issue, detailed studies of the energy balance and energy flows during runaway plateau plasma termination are scarce [16, 17, 18]. Experimental evidence for such conversion of magnetic energy into kinetic energy of the

runaway plasma during termination has been reported for the first time in JET [17] where it has been shown that a conversion of a few tenths of the runaway plateau magnetic energy into runaway kinetic energy takes place. However, direct extrapolation of the single-device JET results to ITER is subject to large uncertainties as the conversion of magnetic energy into kinetic energy is affected by plasma characteristics and loss timescales which can depend on the size of the plasma. Therefore, it is necessary to perform a similar analysis to that carried out for JET [17] for various devices with different sizes in order to identify the physical processes determining the magnetic into kinetic energy conversion during the runaway termination phase and its scaling with device size and runaway plateau current magnitude.

In this paper, magnetic to kinetic energy conversion during the termination phase of disruptions with runaway plateau formation in JET (major radius $R_0 \sim 3$m, minor radius $a \sim 1$m), DIII-D ($R_0 \sim 1.67$m, $a \sim 0.6$m) and FTU ($R_0 \sim 0.935$m, $a \sim 0.30$m) are analyzed and compared. JET discharges include accidental disruptions (most of them before the MK IIA divertor installation) as well as purposely triggered disruptions, typically by puffing a large amount of impurities. The discharges are all in limiter configuration, more favourable to the formation of runaway plateaus [19]. The predisruption plasma current ranges from 1–6MA and the runaway current plateau is in the range of 0.3–3MA. In the case of DIII-D, the disruptions are purposely triggered by argon pellet injection. In most cases, low elongation, inner wall-limited target plasmas are used, as they are found to reliably produce large current plateaus. The pre-disruption plasma current is ~1MA and the observed runaway plateau currents range ~0.05–0.4MA. In FTU, runaway current plateaus are not usually formed after the disruption current quench (less than 5% of cases) [20]. Most of the runaway electron plateaus are observed in disruptions occurring during the flat-top phase of discharges heated with lower hybrid waves or during the current ramp-up phase of ohmic discharges [21]. In addition, in recent experiments, runaway plateaus were purposely triggered by means of neon injection in low density plasmas [22]. The pre-disruption plasma current is ~0.3–0.5MA and the observed runaway plateau currents range ~0.1–0.3 MA).

The paper is organized as follows: In section 2, experimental evidence concerning the characterization of the runaway plasma termination and the conversion of magnetic into runaway kinetic energy in the three devices is presented. In section 3, a zerodimensional model for the termination of the runaway plateau plasma current, including runaway generation and loss, is described and applied to identify the physical mechanisms governing the conversion of magnetic energy into runaway kinetic energy in the various experimental devices. In section 4, a simple model to evaluate the resulting thermal loads by runaway electron impact on plasma facing components is presented and its results compared with JET measurements. Finally, in section 5 modelling of the termination of runaway discharges for ITER (with assumptions derived from the comparison of the models with the experiments from JET, DIII-D and FTU) is presented and the implications for thermal loads on the ITER first wall by runaway electron impact and for their mitigation are discussed.

## 2. BASIC OBSERVATIONS

Figure 2 shows the termination phase of a DIII-D disruption with ~0.25MA runaway current plateau formation. In JET and DIII-D, the main runaway diagnostic providing the data used for the analysis presented in this paper is the hard X-ray emission when the runaway electrons hit the plasma facing components (a description of the hard-X ray diagnostics in JET and DIII-D can be found in Refs. [23] and [24], respectively). In FTU, the standard hard X-ray and neutron monitors [25, 26] practically always saturate during the runaway plateau phase. Therefore, for the present analysis, a low sensitivity U235 fission chamber (with 30 microg/cm$^2$ of U235, 1ms time resolution) has been used: in the runaway plateau phase, this detector is sensitive to hard X-rays (photofissions) and neutrons. The termination phase occurs when, at the end of the plateau phase, the runaway plasma becomes unstable and runaway electrons are lost, often in a series of bursts, in correspondence with the emission of hard X-rays or the photoneutron emission produced when the electrons impinge on the plasma facing components [27, 9]. The processes that lead to the runaway plateau instability, such as movement of the plasma column leading to compression of runaway plasma against the wall and triggering MHD instabilities [27], MHD instabilities of the runaway beam itself [28], etc, are not well understood. The duration of the runaway loss during the termination phase, $\Delta t_{hxr/neut}$, in JET, DIII-D and FTU disruptions is evaluated as the time interval between the abrupt increase in the hard X-ray emission or photoneutron emission and the disappearance of any such signal. Note that already during the plateau phase (after the current quench) the hard X-ray and photoneutron emission is higher than in the pre-disruption phase, due to in-plasma bremsstrahlung of circulating runaway electrons and to thick-target bremsstrahlung interactions with the plasma facing components of runaway electrons that are slowly diffusing out of the plasma. $\Delta t_{hxr/neut}$ is plotted in Fig. 3 versus the plateau runaway current, $I_0$ (i.e., the value of the current during the plateau phase of the disruption), for the three devices, ranging typically from 1 to 10ms and showing no clear correlation with device size or with the magnitude of $I_0$. In the case of JET, disruptions before (mostly accidental) and after the MK-IIA divertor installation (most of them purposely triggered) are indicated separately in this figure. For the case of DIII-D, discharges in which the runaway plasma is terminated together with the loss of vertical or horizontal position are also indicated separately in this figure. During the runaway loss period, $\Delta t_{hxr/neut}$, the plateau current, $I_0$, initially carried by the runaway electrons, decreases and converts into resistive current in the residual ohmic plasma which surrounds the runaway beam until, once all the runaways have been lost, all the plasma current, $I_p$, is ohmic, $I_{aft} \equiv I_p (t = \Delta t_{hxr/neut})$, and resistively decays to zero, i.e., the final termination of the disruption with runaway plasma formation (see top Fig.2). It is during $\Delta t_{hxr/neut}$, when the runaway electrons are being lost, that additional conversion of magnetic energy into runaway kinetic energy may occur due to the decay of the plasma current. The decrease of the plasma current yields an inductive electric field which can accelerate the existing runaways or even generate new runaway electrons. At the same time, a resistive current is induced in the plasma ($E_{||} = j_{OH}$; $j_{OH}$ is the ohmic current density) which can ohmically dissipate part of the magnetic energy. The balance between these two opposite effects will determine to a great extent

the final energy fluxes in the form of runaway electrons onto the plasma facing components.

The residual resistive current, Iaft, after the runaway electrons are lost must be correlated, due to the physics picture above, with the ohmic dissipation during the current termination phase. In Fig.4, $I_{aft}$, normalized to $I_0$, is plotted versus $\Delta t_{hxr/neut}$ for the three devices (JET, DIII-D and FTU). Even though $I_{aft}/I_0$ shows a large variability (typically > 20% in JET, > 50% in DIII-D vertical losses, ~0 – 100% for DIII-D midplane losses, and < 40% in FTU), this figure supports a correlation of $I_{aft}$ with $\Delta t_{hxr/neut}$. The largest $I_{aft}/I_0$ ratios correspond to the shortest runaway terminations; the faster the runaway electrons are lost, the larger is the inductively generated electric field ($E_{||} \propto dI_p/d_t$) and, hence, the resulting ohmic current. Furthermore, the physics picture above suggests a correlation between $I_{aft}$ and the resistive decay time of the ohmic current circulating in the residual plasma when the runaway electrons are lost, $\tau_{res} \equiv L/R_p$, where L and $R_p$ are the plasma inductance and resistance, respectively. During the runaway loss phase the electric field can be approximated by $E_{||} = \eta\, j_{OH} \sim (L/2\pi R_0)\, |dI_p/dt|$. Approximating $j_{OH} \sim I_{aft}/\pi a^2$, $|dI_p/dt| \sim (I_0 - I_{aft}) = \Delta t_{hxr/neut}$, results in

$$\frac{I_{aft}}{I_0} \sim \frac{\left(\tau_{res}/\Delta\, t_{hxr/neut}\right)}{1 + \left(\tau_{res}/\Delta\, t_{hxr/neut}\right)} \tag{4}$$

In the experiment, it is not possible to determine the resistive decay time of the residual ohmic plasma in the runaway plateau phase as all the plasma current is carried by the runaways themselves. Therefore, the resistive time, $\tau_{res}$, has been inferred from the decay of the plasma current after the runaways are lost; i.e. after $\Delta t_{hxr/neut}$ when all the current circulating in the plasma is ohmically driven. The resistive decay time, $\tau_{res}$ is thus $\tau_{res} \equiv I_{aft}/|dI_p/dt|_{aft}$, where $|dI_p/dt|_{aft}$ is the current derivative after $\Delta t_{hxr/neut}$. Figure 5 shows $\tau_{res}$ versus the plateau runaway current, $I_0$, in DIII-D, JET and FTU. In general res is larger for JET plasmas than for the smaller devices. The lack of size scaling between DIII-D and FTU can be attributed to the fact that in the DIII-D experiments the runaway plasmas are formed by the injection of Ar pellets which unavoidably leads to low plasma temperatures in the residual ohmic plasma and thus to unusually short resistive times. On the contrary, FTU runaway experiments correspond to low/medium density disruptions in the ramp-up or with LHCD heating which favour higher plasma temperature in the residual ohmic plasma and thus relatively long resistive times for its size.

As illustrated in Fig.6 and in agreement with the physics picture introduced in this section, a clear correlation between $I_{aft}/I_0$ and $\tau_{res}/\Delta t_{hxr/neut}$ is indeed found among all experiments, which is consistent with the phenomenological relation (4) (full line in the figure). Moreover, as it will be demonstrated in Sec. 3, such a correlation is also supported by theory.

Although it is not possible to determine the current profile evolution during the runaway loss phase, Δthxr=neut, it is not likely that the current profile of the ohmic plasma after the runaway loss is more peaked than the initial runaway plateau plasma [17], i.e., $L_r \geq L_{aft}$, where $L_r$ and $L_{aft}$ are the inductances of the runaway plateau plasma and the ohmic plasma after $\Delta t_{hxr/neut}$, respectively. Accordingly, a lower estimate of the magnetic energy dissipated during $\Delta t_{hxr/neut}$ can be obtained:

$$\frac{\Delta W_{mag}}{W^0_{mag}} \equiv \frac{W^0_{mag} - W^{aft}_{mag}}{W^0_{mag}} \geq 1 - \left(\frac{I_{aft}}{I_0}\right)^2 \quad (5)$$

($W^0_{mag}$, $W^{aft}_{mag}$ are the magnetic energies of the plateau and ohmic plasma after $\Delta t_{hxr/neut}$, respectively).

This lower bound on $\Delta W_{mag}/W^0_{mag}$ is shown in Fig.7 versus $\tau_{res}/\Delta t_{hxr/neut}$ indicating that a significant fraction of the initial magnetic energy of the runaway plateau plasma can be lost within the runaway loss period for a significant number of disruption terminations, reaching up to ~100% dissipation at the lowest values of $\Delta t_{hxr/neut}$. The energy balance analysis performed in [17] on JET disruptions showed that the radiation losses during the whole runaway current termination phase are typically small as well as the losses associated with the induction of currents on the vessel. As a result, most of the magnetic energy of the runaway plasma will be directly deposited onto the plasma facing components either by direct deposition of the runaway electron kinetic energy or by conduction/convection of thermal energy in the residual ohmic plasma. The total energy deposited by the runaway electrons will be the sum of the initial kinetic energy in the runaway beam plus the magnetic energy converted into runaway kinetic energy during the runaway loss period, while the thermal plasma energy will mostly correspond to the ohmic dissipation during the whole termination phase. The question is, thus, how large the conversion of magnetic energy into kinetic energy of the runaways is.

A rough estimate can be obtained directly from the experiment by assuming that the integral of the hard X-ray emission (HXR) over $\Delta_{thxr}$ must be proportional to the total kinetic energy of the runaway beam, $\int \Delta_{thxr} HXR \sim W_{run}$. In addition, a discharge at low $\Delta_{thxr}$, for which no conversion of magnetic into kinetic energy is expected (~100% conversion into ohmic current) is taken as reference for normalization. Thus for this reference discharge $W_{ref} \sim (\int \Delta_{thxr} HXR)_{ref} \sim W^0_{ref}$, where $W^0_{ref}$ is the kinetic energy of the runaway plateau plasma before the loss phase. With this methodology, an experimental estimate of the increase in the total runaway kinetic energy during the termination of a disruption can be obtained as

$$\left(\frac{W_{run}}{W^0_{run}}\right)_{HXR} \sim \frac{W_{run}}{(I_0/I^0_{ref})\, W^0_{ref}} \sim \frac{\int_{\Delta t_{hxr}} HXR}{(I_0/I^0_{ref})\, \left(\int_{\Delta t_{hxr}} HXR\right)_{ref}} \quad (6)$$

where it has been assumed that the kinetic energy of the runaway plateau plasma, $W^0_{run}$, must be proportional to $I_0$ [29], $W^0_{run} \sim (I_0/I^0_{ref}) W^0_{ref}$.

The results of the application of such approach are shown in Fig.8 for DIII-D (top) and JET discharges before divertor installation (bottom) versus $\Delta^t_{hxr}$. The results from DIII-D thus indicate that a significant (up to ~10×) conversion of runaway magnetic energy to runaway kinetic energy is occurring for sufficiently slow losses. For rapid losses, the runaway plasma magnetic energy appears to go mostly into the induction of current into the residual ohmic plasma. In the case of JET discharges before divertor installation, a behaviour similar to that observed in DIII-D is inferred. Further experimental support for conversion of magnetic into runaway kinetic energy is coming

from heat load measurements due to runaway electrons onto the JET upper dump plate, where the surface temperature increase on the CFC tiles is found to scale with the square of the runaway current [30] (see section 4 for a more detailed discussion).

## 3 MODELING AND IDENTIFICATION OF ENERGY CONVERSION MECHANISMS

### *3.1 THE MODEL*

In order to confirm the above picture and to understand in detail the physical mechanisms that govern the conversion of magnetic energy into energy deposited onto the plasma facing components during the termination of runaway plasmas, with a view to their evaluation for ITER, modeling of the JET, DIII-D and FTU termination phases has been performed. A zero dimensional model of the termination phase including the generation of runaways has been applied, which is similar to the model used in [31] for the analysis of runaway generation in TEXTOR disruptions. The model takes into account the primary and secondary runaway generation mechanisms, the loss of the runaway electrons with a characteristic timescale, $\tau_{diff}$ , and the replacement of the runaway current by the ohmic current during the phase in which the runaway electrons are lost. The induced currents in the vessel are also included in the model and, hence, the dissipation of magnetic energy by ohmic currents in the vessel as well as the penetration of external (to the vessel) magnetic energy through the vacuum vessel during the runaway termination phase. There exist more sophisticated models dealing with runaway electrons like onedimensional codes [13, 21] or kinetic approaches [12]. However, despite being simple, the model used in this paper is able to capture the physics processes essential to the problem and provide an appropriate description of the magnetic energy conversion during the runaway termination phase with fewer free parameters than these codes. The more sophisticated modelling codes require detailed knowledge of density, temperature and current density profiles during the runaway termination phase which are not available in the experiment.

In our simple model, the termination phase of the runaway plasma is described by three equations: an equation for the plasma current, $I_p$, an equation for the current induced in the vessel, $I_v$, and an equation for the runaway current, $I_r$, generation and loss:

$$\frac{d}{dt}(L_p I_p + M I_v) = -2\pi R_0 E_{||} \tag{7}$$

$$\frac{d}{dt}(M I_p + L_v I_v) = -I_v R_v \tag{8}$$

$$\frac{d}{dt}(M I_p + L_v I_v) = -I_v R_v \tag{9}$$

Here $I_p = I_r + I_{OH}$ ($I_{OH}$ is the ohmic current), and $L_p$ is the total plasma inductance, $L_p \equiv L_{int} + L_{ext}$, where $L_{int}$ and $L_{ext}$ are the internal and external plasma inductances, respectively, given by $L_{int} \equiv \mu_0 R_0 \, l_{int}/2$ and $L_{ext} \equiv \mu_0 R_0 \, (\ln(8R_0/a) - 2)$. M and Lv are the mutual plasma - vessel inductance and the vessel inductance, respectively, $M \approx L_v \approx L_{ext}$, and $R_v$ is the vessel resistance, which determines

the vessel resistive time, $\tau_v \equiv L_v/R_v$. In this study we have used a simple model of the vessel as a whole and, therefore, $\tau_v$ has been computed with the effective inductance and resistance of the vessel itself as well of its conducting internal structures. These effective parameters have been evaluated from the inductances, resistances and mutual inductances of the vessel and the internal conducting structures following a procedure similar to that in [33]. Coupling and energy transfer to the PF coils or other ex-vessel passive conducting structures is not included in our analysis. This would require a detailed simulation of the circuits for each machine [32, 33] which is beyond the scope of this paper. Previous calculations have shown that the current density profile and, therefore, the internal plasma inductance change during the formation and the termination of the runaway plasma, increasing during the current quench [12, 13] and decreasing during the termination phase of the disruption [17]. These effects cannot be described by the zero-dimensional model used in the present study but it will be included in future more detailed studies with a 1-D model for runaway generation and loss similar to that developed for [17].

The first contribution to $dI_r/d_t$ in Eq. (9) describes the Dreicer generation,

$$\left(\frac{dI_r}{dt}\right)_{Dreicer} \approx ec \left(\frac{dn_r}{dt}\right)_{Dreicer} S, \tag{10}$$

where $(dn_r/d_t)$Dreicer is the Dreicer runaway generation rate [34] and S the plasma cross section. The second term in Eq. (9) corresponds to the avalanche (secondary) runaway generation mechanism,

$$\left(\frac{dI_r}{dt}\right)_{avalanche} \approx \frac{I_r}{\tau_s}, \tag{11}$$

with $\tau_s$, is the characteristic avalanching time [15, 16], given by,

$$\tau_s \approx \frac{4\pi\varepsilon_0^2 m_e^2 c^3}{e^4 n_e} \sqrt{\frac{3(5 + Z_{eff})}{\pi}} \left(\frac{E_{||}}{E_R} - 1\right)^{-1}, \tag{12}$$

where $E_R = n_e e^3 \ln\Lambda/4\pi\varepsilon_0^2 m_e c^2$ is the critical field for runaway generation [34, 15] and the electric field, $E_{||}$, is determined by the resistive current in the plasma,

$$E_{||} = \eta j_{OH} = \eta (j_p - j_r). \tag{13}$$

is the plasma resistivity, and $j_{p,r}$ the plasma and runaway current densities, respectively ($j_{p,r} \simeq I_{p,r}/S$). Finally, the third term describes the loss of runaway electrons with characteristic timescale $\tau_{diff}$.

The magnetic energy deposited on the runaway electrons, and that ohmically dissipated in the plasma and the vessel during the runaway termination phase are provided by:

$$\Delta W_{run} = 2\pi R_0 \int I_r \left(E_{||} - E_R\right) dt \tag{14}$$

$$\Delta W_{OH} = \int I_{OH}^2 R_p \, dt \tag{15}$$

$$\Delta W_v = \int I_v^2 R_v \, dt \tag{16}$$

During the termination phase, the plasma parameters $Z_{eff}$, $n_e$, $T_e$, and therefore the plasma resistivity, $\eta$, are assumed to be constant in this model. Figure 9 illustrates the simulation of the termination phase of a JET runaway plateau plasma of 1MA. The plasma resistive time in this simulation is assumed to be $\tau_{res}$ = 5ms ($T_e \sim 7$eV, $Z_{eff} = 3$) and the diffusion time of the runaway electrons $\tau_{diff}$ = 1ms. The runaway current is lost in a time interval $\Delta t_{hxr/neut} \sim 7$ ms [Fig.9 (a)] during which a significant ohmic current, $I_{OH,max} \sim 0.7$MA, is produced in the residual plasma caused by the induced electric field during the current decay. In these simulations, as the runaway current does not sharply go to zero but decreases more or less exponentially, the time interval for the runaway loss, $\Delta t_{hxr/neut}$, and the residual ohmic current, $I_{aft}$, must be defined as the time and current at which the runaway current has dropped to an appropriately low enough value; typically a fraction ~5% of the initial runaway plateau current, $I_0$, is utilized to define $\Delta t_{hxr/neut}$ for our simulations. For this JET simulation, the maximum induced current in the vessel is ~ 0.2MA, and most of the initial magnetic energy of the runaway plasma is ohmically dissipated in the residual plasma, ~ 2.9 MJ, to be compared with the energy converted into runaway kinetic energy or ohmically dissipated in the vessel, $\Delta W_{run} \sim \Delta W_v \sim 0.45$MJ [Fig.9 (b)].

This modelling procedure has been applied to runaway plasma terminations in JET, DIII-D and FTU, and the results are shown in Fig.10 for the predicted $I_{aft}/I_0$ versus $\Delta t_{hxr/neut}$. In these simulations, the characteristic ohmic decay times, $\tau_{res}$ (typically fitted using $Z_{eff} = 3$ and $T_e \sim 3$, 5 and 12eV for DIII-D, JET and FTU discharges, respectively), and wall times, v, for each device have been used (see Fig.5). It should be noted that $\tau_v$ in JET is different for the two sets of experiments modelled (~8ms before divertor installation and ~4 ms after divertor installation). This is associated with the installation of reinforcement structures for the vacuum vessel and internal divertor components at JET over the ~15 years separating both sets of experiments. Taking into account the typical scattering in the measurements for runaway plasmas, the agreement between modelling and experiment is reasonably good. The major deviation corresponds to DIII-D runaway plasmas which are terminated by a loss of vertical position control (upwards or downwards). In this case, the simulations lie well below the experiment and a larger ohmic decay time in the model (~3ms) instead of the measured one (~1.6ms) has to be used to reconcile modelling predictions and experimental measurements. It is not presently understood if this discrepancy can be attributed to the rapid vertical motion of the plasma and associated changes in the mutual plasma-vessel inductance, which are not considered in our simple 0-D model, or to a different nature of the plasmawall interaction for rapid runaway strikes against the DIII-D upper and lower divertor plates. It is nevertheless important to note that, for the simulations with $\tau_{res}$ ~3ms, the predicted induced currents in the vessel at runaway

termination are in good agreement with the measured values $I_v/I0 \sim 40\%$ [35], which indicates that the discrepancy between model and experiment is probably linked to the variation of the plasma-vessel mutual inductance caused by the vertical movement of the plasma as the runaway electrons are lost.

The calculated magnetic energy converted into runaway kinetic energy (normalized to the initial runaway plateau plasma internal magnetic energy, $W^0_{mag.int} = L_{int} I_0^2/2$) during runaway termination, $\Delta W_{run}/W^0_{mag,int}$, for the simulations of Fig.10, is shown in Fig.11 versus the runaway loss time. The conversion of magnetic into runaway kinetic energy increases with $\Delta t_{hxr/neut}$, consistent with the decrease of $I_{aft}/I_0$ and the experimental observations presented in Fig.8. The energy deposition onto the runaways is predicted to be lower for JET, which is also consistent with the observed increase of $I_{aft}/I_0$ with $\tau_{res}/\Delta t_{hxr/neut}$ (see Fig.6) and the larger ohmic decay times in the JET device. Values larger than one for ΔWrun=W0mag;int are associated with the penetration of external magnetic energy across the vacuum vessel, due to its finite resistivity, and secondary runaway electron generation during the runaway termination phase, which will be described in more detail later in this section.

Based on these calculations, the total energy that is deposited by the runaway electrons, Wrun (including the plateau runaway beam kinetic energy) onto the plasma facing components, normalized to the plateau kinetic energy, $W^0_{run}$, is given by

$$\frac{W_{run}}{W^0_{run}} = \frac{W^0_{run} + \Delta W_{run}}{W^0_{run}} = 1 + \frac{W^0_{mag,int}}{W^0_{run}} \left( \frac{\Delta W_{run}}{W^0_{mag,int}} \right) \approx 1 + \alpha I_0 (MA) \left( \frac{\Delta W_{run}}{W^0_{mag,int}} \right) \quad (17)$$

$$\alpha \approx \frac{150 L_{int} (\mu H)}{2\pi R_0 (m) E_{av} (MeV)} \quad (18)$$

where $W^0_{mag,int}$ is the internal magnetic energy of the plasma and the plateau runaway beam energy has been approximated as

$$W^0_{run} \approx N_r E_{av} \approx \frac{2\pi R_0 I_0}{e c} E_{av}$$

($E_{av}$ is the average individual runaway electron kinetic energy in the plateau).

A comparison of $W_{run}/W^0_{run}$ calculated (for several values of $E_{av}$) using Eq. (17) and the predicted $\Delta W_{run}/W^0_{mag,int}$ from Eq. (14) (Fig.11) with the estimates made in DIII-D and JET (before divertor installation) based on HXR emission measurements (Fig.8) is shown in Fig.12. The calculations match reasonably well the HXR-based estimates (although the scattering is large in the case of JET) when an average kinetic energy for the individual runaway electrons $E_{av} \sim 0.50$MeV in DIII-D, and $E_{av} \sim 4$MeV for JET are assumed. These runaway energy values required by the model for DIII-D and JET to match the measurements are consistent with recent observations both in DIIID and JET. In DIII-D, the measured distribution function of the runaways appears to be skewed towards low energies [35], while at JET runaway distributions typically have average energies of a few MeVs with significant runaway populations up to ~ 10MeV [36].

### *3.2 ENERGY CONVERSION MECHANISMS*

*3.2.1 Acceleration of the plateau runaway electrons*

Once it has been shown the consistency of the simple modelling described by Eqs.(7)–(9) with the experimental observations in DIII-D, JET and FTU, it is now necessary to proceed with a more detailed analysis of the mechanisms determining the conversion of magnetic into runaway kinetic energy. This is of particular interest for the extrapolation of these results to future devices such as ITER because of the different scaling of the various processes involved with the size of the device and the vacuum vessel electrical properties. We will start with a zero order approximation, in which the runaway plasma energy gain from the collapse of its magnetic energy is assumed to be only due to acceleration of the plateau runaway electrons by the induced electric field during the decay of the current, and effects associated with the generation of runaways or with the coupling of the plasma current to the vacuum vessel will be neglected. Under such assumptions, Eqs.(7)–(9) can be simplified to the set of equations

$$\frac{d}{dt}\left(L_{int}\, I_p\right) \approx -\, 2\pi R_0 E_{||} \tag{19}$$

$$\frac{dI_r}{dt} \approx -\, \frac{I_r}{\tau_{diff}}, \tag{20}$$

with $E_{||} = \eta\,(j_p - j_r) \approx \frac{\eta}{\pi a^2}\,(I_p - I_r)$. These equations can be solved analytically yielding

$$I_p(t) \;=\; \frac{I_0\,\tau_{res}}{\tau_{res} - \tau_{diff}}\left(e^{-t/\tau_{res}} - \frac{\tau_{diff}}{\tau_{res}}\, e^{-t/\tau_{diff}}\right) \tag{21}$$

$$I_r(t) \;=\; I_0\, e^{-t/\tau_{diff}} \tag{22}$$

This approximation thus provides analytical estimates for the magnitude of the residual ohmic current, $I_{aft}$, after the runaways are lost, and for the kinetic energy, $\Delta W^{0}_{mag,int}$, gained by the runaway beam at runaway plasma termination. As explained above, due to the exponential time decay of the runaway current in the model, the duration of the runaway loss, $\Delta t_{hxr/neut}$, and the residual ohmic current, $I_{aft}$, must be defined as the time and current when the runaway current has dropped to a small enough fraction (typically, $f \sim 5\%$) of the initial plateau current:

$$f \;\equiv\; \frac{I_r(\Delta\, t_{hxr/neut})}{I_0} \;=\; e^{-\Delta\, t_{hxr/neut}/\tau_{diff}} \Rightarrow \Delta\, t_{hxr/neut} \;=\; -\tau_{diff}\;\; ln f$$

Using this definition and Eq.(21) one obtains,

$$\frac{I_{aft}}{I_0} \equiv \frac{I_p\,(\Delta\, t_{hxr/neut})}{I_0} \;=\; \frac{R}{R-1}\left(f^{\,1/R} - \frac{f}{R}\right) \tag{23}$$

where

$$R \equiv \frac{\tau_{res}}{\tau_{diff}} \approx \frac{a^2 L_{int}}{2R_0 \eta \tau_{diff}} \tag{24}$$

Similarly, the kinetic energy gained by the runaways will be given by [Eq.(14)], which can be written as

$$\Delta W_{run} = 2\pi R_0 \int_0^\infty I_r \left(E_{||} - E_R\right) dt = R_p \int_0^\infty I_r \left(I_p - I_r\right) dt - 2\pi R_0 \int_0^\infty I_r E_R \, dt \tag{25}$$

Substituting Eqs. (21), (22) for $I_p(t)$ and $I_r(t)$, respectively, and integrating leads to the following analytical expression for the conversion of runaway magnetic energy into runaway kinetic energy:

$$\frac{\Delta W_{run}}{W^0_{mag,int}} = \frac{1}{1+R} - \frac{4\pi R_0 E_R}{I_0 R_p} \frac{1}{R} \tag{26}$$

For the disruptions considered here, collisional runaway dissipation is expected to be negligible (for $n_e = 5\times10^{20}\,m^{-3}$, $E_R \sim 0.5$V/m, which is much smaller than the estimates of $E_{||}$ during the termination phase). In this case, Eq. (26) can be simplified to

$$\frac{\Delta W_{run}}{W^0_{mag,int}} \approx \frac{1}{1+R} \tag{27}$$

Both Eq. (23) and Eq. (27) contain $R \sim \tau_{res}/\tau_{diff}$ as the fundamental parameter determining the conversion of runaway current into ohmic current, $I_{aft}$, and the conversion of magnetic energy deposition into runaway kinetic energy. With increasing R, the efficiency of the magnetic energy conversion into runaway kinetic energy decreases. This result is illustrated in Fig.13, in which the analytical approximation (23) for $I_{aft}/I_0$ is compared with the experimental measurements showing an excellent consistency with the experiment.

It should be, however, noted that, as runaway generation and coupling to the vessel have been neglected, the conversion of magnetic into runaway kinetic energy, $\Delta W_{run}$, can be underestimated in the approximation leading to Eq. (27). In Fig.14, the results of the simplified analytical model for $\Delta W_{run}/W^0_{mag,int}$ versus $\tau_{res}/\tau_{diff}$ [Eq. (27)] are compared with the numerical results of the full model [Eqs. (7)–(9)] applied to JET, DIII-D and FTU terminations (Fig.10 parameters). It is inferred from the figure that, while ΔWrun is well described by the simplified analytical model at high values of $\tau_{res}/\tau_{diff}$ (fast terminations), effects associated with runaway generation and coupling to the vessel can increase the fraction of magnetic energy converted into runaway kinetic energy for slow terminations (low enough $\tau_{res}/\tau_{diff}$ values), which can reach values larger than 1 for the conversion of the internal magnetic energy of the runaway plasma into kinetic energy of the runaways.

*3.2.2 Runaway generation*

The acceleration of runaway electrons generated during the termination phase of the current can

increase the fraction of the plateau magnetic energy that can be converted into runaway kinetic energy. The induced electric field during the runaway termination phase is typically lower than during the initial current quench in the disruption, which leads to the formation of the runaway plasma plateau, mainly due to the smaller plasma current. Therefore, due to the exponential dependence of the Dreicer mechanism on the electric field, much lower runaway production by this mechanism would be predicted at the runaway termination phase compared with the initial current quench phase of the disruption. It is thus expected that the main runaway generation mechanism during the runaway termination phase, in particular for large devices, will be the avalanche mechanism.

Figure 15 shows the effect of the secondary runaway generation for the JET, DIII-D and FTU runaway terminations. In this figure, for the same parameters than Fig.10, the results of the full numerical model (which includes avalanche runaway generation) for $\Delta W_{run}/W^{0}_{mag,int}$ versus $\tau_{diff}$ (full line) are compared with those obtained without including the avalanche generation of runaways (dashed line). The effects of avalanche are observed to increase with the device size (magnitude of the current), being small or negligible in DIII-D and FTU but noticeable already for JET. The role played by avalanche generation is also found to be larger for slow terminations even if, in these cases, the induced electric field and, hence, the secondary runaway growth rate, is smaller. The reason for such a behaviour is that the drop in the avalanche growth rate when diff increases is smaller than the reduction in the runaway loss rate itself so that the net result is an increase in the number of runaway electrons during the termination phase.

While, in the absence of avalanche, the conversion of magnetic energy into runaway kinetic energy is only due to the energy gain of the plateau runaway electrons in the induced electric field, secondary generation of runaway electrons increases its number, so that energy conversion is the result of both runaway density and energy increase during the plateau termination phase, which results in a larger conversion efficiency. The avalanche growth of the runaway electrons (normalized to the plateau runaway population), for the same terminations and parameters than Fig.10, is illustrated in Fig.16. This is estimated by integration of the avalanche runaway growth rate during the current termination phase,

$$(\Delta I_r)_{av} \approx \int \frac{I_r}{\tau_s}\, dt = \frac{e\ \Delta W_{run}}{(2\pi R_0)\,(m_e c)\ln\Lambda\ a(Z_{eff})},$$

where Eq.(12) has been used for $\tau_s$ and $\Delta W_{run} = 2\pi R_0 \int I_r\,(E_{\|} - E_R)\,dt$, which, normalizing to the plateau runaway population, yields

$$\frac{\Delta N_r^{av}}{N_0} \equiv \frac{(\Delta I_r)_{av}}{I_0} \approx \frac{e\ \Delta W_{run}}{(2\pi R_0)\,(m_e c)\ln\Lambda\ a(Z_{eff})\, I_0} \qquad (28)$$

As expected, the avalanche runaway growth in Fig.16 increases with diff and the device size and, in the case of JET, may become larger than 100% of the initial runaway plateau population.

The effects of avalanche generation for the termination phase are also noticeable in the

duration of the runaway loss period. To quantify this, we define the loss time of runaways for the case in which there is only runaway acceleration (i.e. no avalanche; exponential decay of $I_r$) as $\tau_{exp} \equiv -\tau_{diff} \ln f$ and compare it to the runaway loss time $\Delta t_{hxr/neut}$, numerically calculated, which includes runaway generation. The results are shown in Fig.17, with avalanche runaway generation resulting in a longer runaway loss time interval than that due to acceleration and diffusion of runaways alone. It is important to note that $\Delta_{hxr/neut}/\tau_{exp}$ is always close to one for DIII-D and FTU, but it increases substantially above one in JET for slow runaway terminations, for which secondary generation becomes sizeable.

Besides the numerical results shown in Fig.17, it is possible to get a simple analytical estimate for the increase in runaway deposition timescale ($\Delta t_{hxr/neut}$) due to the effect of avalanche runaway generation. If Dreicer generation as well as collisional runaway dissipation are neglected, Eq. (9) for $I_r(t)$ simplifies to

$$\frac{dI_r}{dt} \approx I_r \left( \frac{1}{\tau_s} - \frac{I_r}{\tau_{diff}} \right) \approx - I_r \left( \frac{e L_{int}}{2\pi R_0 m_e c \ln\Lambda \, a(Z_{eff})} \frac{dI_p}{dt} + \frac{1}{\tau_{diff}} \right)$$

($\tau_s \approx m_e c \ln\Lambda \, a(Z_{eff}) = eE_{\|}$, with $a(Z_{eff}) = \sqrt{3\,(5 + Z_{eff}) = \pi}$ and $E_{\|} \approx -L_{int}\dot{I}_p = 2\pi R_0$), which can be solved analytically yielding

$$I_r = I_0 \, e^{G(I_p)} \, e^{-t/\tau_{diff}} \tag{29}$$

where

$$G(I_p) \equiv \frac{eL_{int} \, (I_0 - I_p)}{(2\pi R_0)\,(m_e c) \ln\Lambda \, a(Z_{eff})}$$

is the runaway avalanche amplification gain factor.

Defining, as above, $\Delta t_{hxr/neut}$ and $I_{aft}$ as the time and current when Ir has dropped to a small enough fraction, $f$, of $I_0$, $f \equiv I_r(\Delta t_{hxr/neut}) / I_0$ , from Eq. (29), it is obtained

$$\Delta t_{hxr/neut} = \tau_{exp} + \frac{eL_{int} \, I_0}{(2\pi R_0)\,(m_e c) \ln\Lambda \, a(Z_{eff})} \, \tau_{diff} \left( 1 - \frac{I_{aft}}{I_0} \right) \tag{30}$$

where $\tau_{exp} \equiv -\tau_{diff} \ln f$ is the exponential decay time of $I_r$ when no avalanche is considered and the second term represents the increase in $\Delta t_{hxr/neut}$ due to the secondary generation of runaways. The effects of runaway generation on the runaway deposition timescale increase with the magnitude of the plateau current, $I_0$, as well as for slow terminations, for which $I_{aft}/I_0$ is small, in agreement with the full model results shown in Fig. 17.

*3.2.3 Vessel coupling and eld penetration*

The magnetic energy of the runaway plateau plasma current, $W_{mag} = L_p I_0^2/2$, can be divided into inside and outside the conducting wall, ($L_p = L_{int} + L_{ext}$). During the runaway termination phase, the external energy diffuses into the vacuum vessel on a characteristic time scale $\tau_v \equiv L_v/R_v$. Therefore,

if the loss of the runaways occurs in a time scale similar or longer than v, a fraction of the external magnetic energy, in addition to the internal magnetic energy, can also be converted into runaway plasma kinetic energy.

Two limiting cases can be considered for the diffusion of the external magnetic energy: a perfectly conducting vacuum vessel or a perfectly resistive vacuum vessel. For a perfectly conducting vacuum vessel , $R_v \rightarrow 0$ ($\tau_v \rightarrow \infty$) and thus

$$\frac{d}{dt}(I_p + I_v) = -\frac{I_v}{\tau_v} \rightarrow 0 \Rightarrow \frac{d}{dt}((L_p - M)\, I_p) \equiv \frac{d}{dt}(L_{int}\, I_p) = -2\pi R_0 E_{||},$$

so that the total current in the plasma ($I_p = I_r + I_{OH}$) decays with the internal plasma inductance, Lint, and no external magnetic energy diffuses through the wall. In the limit of an infinitely resistive vacuum vessel ($R_v \rightarrow \infty, \tau_v \rightarrow 0$), the induced current in the vessel would be zero and, hence, from Eq. (7), the plasma current would evolve with the total plasma inductance, $L_p = L_{int} + L_{ext}$,

$$\frac{d}{dt}(L_p I_p) = -2\pi R_0 E_{||},$$

The reality is an intermediate case between these two limiting cases. In the initial phase of the runaway termination, the vessel behaves as a perfectly conducting vessel and the plasma current decays with an inductance of $L_{int}$ while, at later times, for sufficiently long terminations, the vessel behaves as a resistive one and the plasma current decays with an inductance of $L_{int} + L_{ext}$. Figure 18 illustrates the effect of field penetration through the vacuum vessel for the JET, DIII-D and FTU runaway terminations considered in this study. The results of the simulations for these discharges are compared with the perfectly conducting and resistive vessel cases ($\tau_v \rightarrow \infty$ and $\tau_v \rightarrow 0$, respectively) for the same plasma parameters. The vertical dashed lines indicate the typical range for $\Delta t_{hxr/neut}$ measured in each device. The penetration of the external magnetic energy (finite $\tau_v$) increases the kinetic energy gained by the runaway plasma in comparison with the perfectly conducting case ($\tau_v \rightarrow \infty$). The more resistive (lower $\tau_v$) the vessel and the slower the runaway plasma terminations are, the larger this gain is. DIII-D and JET (after divertor installation) ($\tau_v \approx 8$ms) runaway terminations are close to the perfectly conducting limit, although for the slowest DIII-D terminations (with $\Delta t_{hxr/neut} >> \tau_v$), the increase in ΔWrun=W0 mag;int becomes noticeable (~30% for $\Delta t_{hxr/neut}$ ~20ms). JET (before divertor installation) runaway terminations ($\tau_v \approx 4$ms) are close to the perfectly resistive limit although, for the measured runaway loss time intervals, the effects due to the penetration of the external magnetic energy are not significant. FTU terminations show the largest effects, with a substantial increase in the kinetic energy gained by the runaway electrons for the whole measured range of $\Delta t_{hxr/neut}$. This is due to the very short vacuum vessel penetration time in FTU ($\tau_v \approx 1$ms).

## 4. RUNAWAY HEAT LOADS ON THE PLASMA FACING COMPONENTS

The analysis of experimental measurements carried out in JET, DIII-D and FTU and its comparison with modelling has shown that substantial conversion of magnetic energy into runaway kinetic energy can take place during the termination phase of a runaway plateau plasma, particularly for

slow terminations. For the evaluation of possible consequences to plasma facing components of this runaway kinetic energy deposition, it is necessary not only determine the magnitude of the deposited energy but also the timescale of energy deposition. As an example, Fig.19 (top) shows the calculated power loads due to the deposition of runaways, Pr(t) (energy deposited by the runaways / time), during termination of a 1MA JET runaway current plateau, for typical parameters of experiments carried out at JET after the installation of the divertor ($\tau_{res}$ = 2.5ms; $\tau_v$ = 8ms) and assuming a plateau runaway kinetic energy $W^0_{run}$ = 0.5MJ [37]. In the case of fast terminations, the total deposited energy is only the initial runaway plateau plasma kinetic energy and the fraction of the magnetic energy converted into runaway kinetic energy is small; due to the short deposition timescales, the peak deposited power by runaways is large. For slow terminations, the peak power load is much lower but the plasma facing components are exposed to this power flux for a much longer timescale. In these slow terminations. the total amount of energy deposited by runaways is larger than for short terminations due to the conversion of magnetic into runaway energy.

The increase of the surface temperature of the plasma facing components under runaway impact can be approximately evaluated by the application of the one-dimensional solution of the heat diffusion equation in a semi-infinite solid [38] and taking into account that the runaway electrons, because of the high energies in the MeV range, have a nonnegligible penetration depth. Assuming an exponential decay of the runaway electron energy deposition into the plasma facing components, the heating at the plasma facing component surface under runaway impact can be evaluated by [39, 19]:

$$\Delta T = \frac{\kappa}{K\delta} \int_0^t q_r(t')\, e^{\kappa (t-t')/\delta^2}\, erfc\left(\frac{\sqrt{\kappa (t-t')}}{\delta}\right) dt', \qquad (31)$$

where $\delta$ is the e-folding length of the heat source caused by runaways into the plasma facing components, $erfc(x) = 1 - \frac{2}{\sqrt{2}} \int_0 e^{-x'^2} dx'$ is the complementary error function, $\kappa = K/\rho c$ (K is the solid heat conductivity, c the heat capacity, $\equiv$ its density), $q_r \equiv P_r/A_w$ is the heat flux density, and $A_w$ the runaway wetted area.

These estimates take only into account the power deposited by the runaway electrons, $P_r(t)$, using the runaway penetration depth, , as an input parameter. This study does not include modelling of the runaway distribution function nor of the ratio of the perpendicular (to the magnetic field) to the parallel runaway energy. These, together with a detailed geometry of the PFCs and of the plasma magnetic configuration should be taken into account for a proper evaluation of the thermal loads by runaway impact on the PFCs [40, 41, 42], which is also beyond the scope of this paper. Fig.19 (bottom) shows the time evolution of the estimated surface temperature rise due to the impact of the runaway beam on a CFC target ($A_w = 1m^2$) with a runaway penetration of $\delta$ = 1mm [19] for the same terminations than the top figure. The largest temperature increase is observed for the longest terminations, when the runaway kinetic energy is deposited with a very long timescale and for which there is significant magnetic to kinetic energy conversion. The effect of the runaway penetration into the solid is illustrated in Fig.20, which compares the maximum value of the temperature increase during the decay of the current as

a function of $\tau_{diff}$ for $\delta$ = 1, 2 and 3 mm, respectively. As a result of runaway electron penetration in the material, the largest temperature increase of the plasma facing components is obtained for the shallowest penetration of runaway electrons and the slowest terminations.

An interesting issue concerning the runaway thermal loads is their scaling with the current plateau and the plateau beam energy. Figure 21 shows sample calculations for $\Delta T$ on the JET CFC upper dump plates versus the plateau runaway kinetic energy, $W^0_{run}$. Calculations have been performed for different values of the characteristic runaway diffusiontime ($\tau_{diff}$ = 0.1; 0.5; 1 and 2ms). The plateau energy, $W^0_{run}$, is taken to be proportional to the runaway current, with a typical value in JET of 0.5MJ for 1MA [37]; $\delta$ = 2mm and the runaway wetted area $A_w = 0.3m^2$ [19, 37]. At low $\tau_{diff}$, the conversion of magnetic into runaway kinetic energy is negligible and, hence, the thermal loads show an approximate linear dependence on $I_0$ and $W^0_{run}$. For increasing $\tau_{diff}$, the energy conversion is stronger and, if $I_0$ is high enough, the magnetic energy conversion dominates the runaway energy loads which will show a trend, for large enough $\tau_{diff}$ and $I_0$, to increase with the square of $I_0$ and $W^0_{run}$. For illustration, Fig.21 also shows the measured temperature increase found in JET due to localized runaway heat loads in disruptions triggered by massive injection of argon and neon [37]. The scaling of the thermal loads with the plateau runaway energy and current supports a sizeable conversion of magnetic into runaway kinetic energy at the termination phase of these runaway plasmas.

## 5. DISCUSSION AND IMPLICATIONS FOR ITER

In this work, an inter-machine comparison of the termination phase of disruptions with runaway current plateau formation has been carried out for three devices (JET, DIII-D and FTU) with substantially different current magnitude and size. Evidence has been found for substantial conversion of magnetic into runaway kinetic energy for slow runaway plasma current terminations. In order to elucidate the dominant energy conversion mechanisms, a comparison has been carried out between these experiments and simple 0-D modeling of the runaway plasma current termination. The results of this comparison indicate that, in present devices, the efficiency of conversion of the runaway plasma magnetic energy into runaway kinetic energy is determined to a great extent by the ratio of the characteristic runaway loss time, $\tau_{diff}$, to the resistive time of the residual plasma after the disruption, $\tau_{res}$. The conversion of magnetic energy into runaway kinetic energy increases with $\tau_{diff}/\tau_{res}$. Secondary runaway generation by avalanche during runaway terminations also leads to an increase in the conversion of magnetic energy into runaway kinetic energy but this is only sizeable for high runaway plasma currents (i.e. mainly for JET) and for long durations of the termination. In addition, penetration of the magnetic energy external to the vacuum vessel has to be taken into account for its conversion into runaway kinetic energy when the timescale of the runaway termination is longer than the vacuum vessel resistive time.

Extrapolations of these experimental results to ITER are subject to large uncertainties mainly associated with our incomplete understanding of the thermal plasma and of the runaway beam

characteristics after the initial current quench phase of the disruption as well as of the instabilities leading to the runaway loss and current termination. Acceptable mechanical loads during disruptions in ITER require that for the majority of the high current (15MA) disruptions, the current quench timescale is in the range of ~50–150ms [43], which is much larger than in actual devices, as expected from the size scaling of the current quench time [4]. The ITER vacuum vessel is a thick double-wall vessel made of stainless steel and, as a consequence, has very low resistivity. This leads to very long timescales for the penetration of the external magnetic energy through it ($\tau_v \approx$ 500ms). These two factors alone, from the analysis performed in Sec.3, would lead to the prediction of a lower efficiency of magnetic energy conversion into runaway kinetic energy in ITER than in present tokamaks. On the other hand, due to the large runaway electron current expected in ITER, the avalanche production of runaway electrons during current termination is more effective and this counter-balances the lower efficiency for magnetic energy conversion into kinetic energy on the basis of the arguments above. The balance of these two opposite trends is illustrated in Fig.22 (top) which shows the fraction of the plateau internal magnetic energy converted into runaway kinetic energy versus the runaway diffusion time, $\tau_{diff}$, for the termination phase of ITER runaway current plateaus in the range of 2 to 10MA ($\tau_{res}$ = 50ms; $\tau_v$ = 500ms). The estimated magnetic to kinetic runaway energy conversion not including secondary electron generation by avalanche in the termination phase (red line) is also shown for comparison. The effects of the avalanche mechanism lead to an increase of the efficiency of magnetic to runaway kinetic energy conversion that, for large currents (10MA) and long terminations ($\tau_{diff}$ = 10ms), can reach a conversion efficiency ~70%. The total energy, $W_{run}$, deposited by the runaway electrons onto the plasma facing components includes both the initial plateau runaway energy, $W_{run}$, and the magnetic to kinetic energy conversion, $\Delta W_{run}$, during the termination of the runaway plasma, i.e., $W_{run} = W^0_{run} + \Delta W_{run}$. Figure 22 (bottom) shows $W_{run}$ as a function of $\tau_{diff}$. For the evaluation of $W^0_{run}$, it is assumed that $W_{run}$ is proportional to $I_0$ and that the average energy of the runaway electrons is $E_{av}$ ~ 15MeV. This corresponds to $W^0_{run}$ ~ 20MJ for a runaway plateau current of $I_0$ = 10MA. Due to the large magnitude of the magnetic energy of the runaway plateau plasma, the magnitude of the magnetic energy converted into runaway kinetic energy can be significant, as much as a few hundreds MJ for large runaway plateau currents and slow terminations. For these simulations the range of diffusion times, $\tau_{diff}$, explored is in the range ~ 0.1 – 10ms, which covers the range observed in the runaway termination experiments in JET, DIII-D and FTU. However, as a consequence of the stronger production of secondary runaway electrons by avalanche during the termination phase in ITER, the total decay time of the runaway current during the termination phase can be substantially larger and can reach values of up to few hundreds ms for slow runaway plasma terminations, as shown in Fig.23 for an initial runaway plateau current of 10MA. It is important to note that the time available for the process of energy conversion to take place might be limited by the timescale of the vertical plasma position instability, which for typical conditions during ITER disruptions is ~ 100ms [43].

Due to the large secondary runaway generation during the termination phase, significant runaway

loads are expected in ITER during termination of runaway plasmas with large currents when compared with present devices as shown in Fig. 24. Using this evaluation for the power deposited by runaways in ITER, the minimum area ($A_{min}$) for runaway deposition which would avoid melting ($\Delta T_{max} \sim 1000K$) of the Be first wall plasma facing components can be estimated, as shown in Fig.25 for various penetration depths of the runaway electrons in Be $\delta = 1$, 2 and 3mm. Present estimates of the runaway wetted area in ITER, on the basis of linear extrapolation of the JET measurements, are in the range of 0.3–0.6$m^2$ [43], which is much smaller than that required for Be melting avoidance for a runaway plateau current of 10MA with an initial (i.e. before termination) kinetic energy of 20MJ. Thus, the results of Fig. 5 confirm the need for significant mitigation of the runaway production during the initial current quench in ITER disruptions if melting of the Be plasma facing components is to be avoided [43].

The dependence of Amin on the plateau current is illustrated in Fig.26 ($\tau_{res} = 50ms$; $\tau_v = 500ms$). The plateau runaway beam energy, $W^0_{run}$, has been assumed proportional to the runaway current, with $E_{av} \sim 15MeV$, and a runaway electron penetration $\delta = 2mm$ is assumed. Collisional runaway energy dissipation is negligible in these simulations ($n_e = 5\times10^{20}$ $m^{-3}$ has been used). For short terminations, $A_{min}$ (and the thermal loads) is approximately proportional to the plateau energy content and, hence, scales linearly with I0. For high runaway currents and long terminations, due to the large magnetic energy of the plateau beam and its conversion into runaway kinetic energy during the termination phase, the resulting power loads on the PFCs increase more strongly than linear with the initial runaway current, $I_0$, and thus the minimum area for Be melting avoidance, $A_{min}$. The horizontal red dashed lines in Fig.26 indicate the estimated range for the runaway wetted area in ITER, $\sim 0.3 - 0.6m^2$ [43].

The present analysis shows that for the conditions modelled, the termination of a runaway plasma with a current $I_0 < 2MA$ would not cause melting of the Be plasma facing components, in agreement with the estimates in [43]. In addition, the results of Fig.26 already indicate the two key parameters that need to be controlled in ITER to avoid Be melting during the termination of runaway plasmas if they are formed: one is the initial kinetic energy of the runaway plasma before its termination, which has to be reduced under the melting threshold for the expected runaway wetted area, and the minimization of the magnetic to kinetic energy conversion.

With the aim of reducing the power loads due to the runaways, thus increasing the range of runaway plateau currents for which melting of the Be plasma facing components can be avoided in ITER for the expected runaway wetted areas, the effect of increasing the electron density during the runaway plateau phase and the plasma resistive time, $\tau_{res}$, have been investigated. Increasing the electron density reduces the secondary runaway electron generation [as $\tau_s \propto (E_{||}/E_R - 1)^{-1}$ and $E_R \propto n_e$] and increases the collisional runaway energy dissipation [$\Delta W_{run} \propto \int I_r (E_{||} - E_R)\, dt$], while longer plasma resistive times, $\tau_{res}$, lead to less efficient conversion of runaway magnetic energy into runaway kinetic energy at termination. Figure 27 compares the evaluated $A_{min}$ estimates for a 5MA runaway plasma termination with $W^0_{run} = 10MJ$ ($E_{av} \sim 15MeV$), $\delta = 2mm$, $\tau_{res} = 50$, 150ms and

$n_e = 5 \times 10^{20}$; $10^{22}$ $m^{-3}$. As shown in this figure, increasing the electron density and/or res reduces the conversion of magnetic into runaway kinetic energy for slow terminations but it is not efficient in controlling the runaway power loads for rapid terminations, which are dominated by the initial kinetic energy content of runaway plateau plasma. During fast terminations, the runaway power loads onto the plasma facing components are found to be roughly proportional to $W^0_{run}$ (see Fig.26), and independent of $\tau_{res}$ and $n_e$. The determination of the timescale for runaway plasma termination in ITER remains uncertain. On the one hand, DIII-D experiments [35] suggest that the velocity of the runaway plasma movement against the plasma facing components influences the timescale of the termination and this movement is very slow in ITER (the typical timescale for the runaway plasma vertical drift is ~ 100ms [43]). On the other hand, the collapse of the runaway plasma in DIII-D is found to take place quickly once a critical minimum diameter (or edge q) of the runaway beam is reached [44]. Depending on the role played by the slow plasma movement in ITER on the triggering of the MHD activity that may terminate the runaway plasma, a range of termination timescales from short (~ a few ms) to long (` hundreds ms) could be expected for ITER. In case of slow enough terminations, the range of runaway plateau currents for which Be melting avoidance can be achieved will increase if the electron density in the runaway plasma is kept to high values (by massive material injection, for instance), as illustrated in Fig. 27. It is important to note that the species used to provide such electron density increase should not decrease the resistive decay time of the ohmic residual plasma under 50ms in order to avoid unacceptable mechanical loads in the initial phase of 15MA disruptions in ITER.

Given the large uncertainties regarding the timescale of the processes leading to the termination of runaway plasmas, avoidance of Be melting by runaway termination in ITER demands a combination of a low enough kinetic energy of the runaway plateau plasma together with a sufficiently high ne and res in order to prevent large conversion of magnetic into runaway kinetic energy. These requirements are quantified in Fig.28 which shows, for a range of runaway plasma plateau currents (3.5, 5, 7.5 and 10MA) and $\delta$ = 2mm, an evaluation of the minimum electron plasma density that would be required to keep $A_{min}$ below ~ 0.6$m^2$ as a function of $\tau_{res}$, for $\tau_{diff}$ = 0.1 – 10ms. In this figure, the plateau runaway beam energy, $W^0_{run}$, is not assumed proportional to $I_0$, but the same and equal to 4MJ for all runaway plateau current levels as $W^0_{run} < 4$MJ is required to ensure that Be melting will not occur for the expected runaway wetted area in ITER of ~ 0.6$m^2$ for the fastest terminations, independently of the plateau runaway current. In the simulations, res has been also kept within the range for acceptable mechanical loads (50–150ms) and densities up to $10^{22}$ $m^{-3}$, which might be achieved by massive gas injection (MGI), have been considered [43].

Figure 28 provides a good guideline for the requirements that need to be met to avoid melting by runaway plasma terminations in ITER. In the first place, as discussed above, the initial kinetic energy of the runaway plateau plasma must be kept at a low enoughvalue, $W^0_{run} < 4$MJ, so that melting does not occur even for fast terminations. In addition, the electron density, as well as res, should be kept at a high level so that the runaway plasma magnetic energy is not converted into

runaway kinetic energy. These are, obviously, very demanding requirements for the highest values of the runaway plateau currents foreseen in ITER but are more likely to be achievable for the lowest runaway current levels and, possibly, they can extend the range of runaway plateau currents for which Be melting is avoided in ITER up to runaway currents of ~ 5MA. On the other hand, the results presented in Fig.28 are based on an estimate of the runaway wetted area in ITER $A_w \sim 0.6m^2$. This is a simple and rough estimate for the runaway wetted area in ITER and more experimental and modelling work is required in order to provide a more sound and physics based estimation of this area, as it is likely to depend on the mechanisms that drive the loss of the runaways themselves. This is a key input required in order to perform a more precise evaluation of the requirements for Be melting avoidance during disruption terminations in ITER than those presented in this paper.

These considerations for mitigation/avoidance of melting of Be plasma facing components in ITER should not be seen as a substitute of the main ITER runaway mitigation strategies, but in addition to them. The main runaway mitigation strategy for ITER remains centered on the avoidance of the generation of large runaway currents by collisional suppression during the current quench or by the degradation of the runaway confinement by controlled magnetic perturbations created by repetitive gas jets [43]. The considerations for the reduction of runaway termination loads on ITER plasma facing components described above should thus be considered as a way to minimize the consequences of such loads if the main mitigation strategy fails to decrease the runaway current to values which lead to a safe termination of the plasma ~ 2MA. The advantage of the line explored in this paper with respect to other runaway mitigation strategies, such as the collisional dissipation of the runaway plateau current and energy by massive gas injection of high-Z impurities [35], is that it does not require the control of the runaway plasma position in ITER over ~ 100ms timescales, which is difficult to achieve in ITER [45]. On the other hand, the line investigated here is limited, by its own nature, to the mitigation of the effects of runaway plasmas termination in ITER to moderate levels of runaway currents (5–7.5MA).

The simple 0-D modelling presented in this paper and its comparison with experimental results from three tokamaks (DIII-D, JET and FTU) has allowed the identification of the physics processes essential to the conversion of magnetic energy into runaway kinetic energy during the termination of disruptions with runaway current plateau formation. This model has also been used to get simple but revealing estimates of the magnitude and timescales of the runaway power fluxes expected during runaway terminations in ITER and it has provided guidelines for their reduction by control of the electron density in the runaway plasma and of the resistive time of the residual ohmic plasma. A more detailed evaluation of the magnitude and consequences of the runaway loads to ITER plasma facing components requires an improved experimental characterization of the runaway population and of the residual ohmic plasma during the runaway plateau phase of the disruption, together with a more sophisticated modelling of the runaway loss processes and of the power loads onto the ITER plasma facing components.

**ACKNOWLEDGEMENTS**

M. Lehnen is thanked for enlightening discussions on runaway electron physics and on the interpretation of the experimental measurements. This work was done under financial support from Dirección General de Investigación y Gestión del Plan Nacional, Project No.ENE2009-12213-C03-03, and Dirección General de Investigación, Científica y Técnica, Project No.ENE2012-31753. This work was supported by EURATOM and carried out within the framework of the European Fusion Development Agreement. The views and opinions expressed herein do not necessarily reflect those of the European Commission or those of the ITER Organization.

**REFERENCES**

[1]. JASPERS, R., LOPES-CARDOZO, N.J., and SCHÜLLER, F.C., Nuclear Fusion **36** (1996) 367.
[2]. WESSON, J.A., et al., Nuclear Fusion **29** (1989) 641.
[3]. YOSHINO, R., Journal of Nuclear Materials **220-222** (1995) 132.
[4]. HENDER, T.C., et al., Progress in the ITER Physics Basis Chapter 2: MHD stability, operational limits and disruptions Nuclear Fusion **47** (2007) S128.
[5]. YOSHINO, R., et al., Plasma Physics and Controlled Fusion **39** (1997) 3113.
[6]. NYGREN, R., et al., Journal of Nuclear Materials **241-243** (1997) 522.
[7]. YOSHINO, R., et al., Nuclear Fusion **39** (1999) 151.
[8]. MARTIN-SOLIS, J.R., SANCHEZ, R., and ESPOSITO, B., Physics of Plasmas **7** (2000) 3369.
[9]. GILL, R.D., et al., Nuclear Fusion **42** (2002) 1039.
[10]. RICCARDO, V., Plasma Physics and Controlled Fusion **45** (2003) A269.
[11]. PLYUSNIN, V.V., et al., Nuclear Fusion **46** (2006) 277.
[12]. ERIKSSON, L.-G., et al., Physical Review Letters **92** (2004) 205004.
[13]. SMITH, H., et al., Physics of Plasmas **13** (2006) 102502.
[14]. JAYAKUMAR, R., et al., Physics Letters A **172** (1993) 447.
[15]. ROSENBLUTH, M.N., et al., Nuclear Fusion **37** (1997) 1355.
[16]. PUTVINSKI, S., et al. Plasma Physics and Controlled Fusion **39** (1997) B157.
[17]. LOARTE, A., et al., Nuclear Fusion **51** (2011) 073004.
[18]. RIEMANN, J., et al., Physics of Plasmas **19** (2012) 012507.
[19]. LEHNEN, M., et al., Journal of Nuclear Materials **390-391** (2009) 740.
[20]. MADDALUNO, G., et al., Journal of Nuclear Materials **266-269** (1999) 593.
[21]. MARTIN-SOLIS, J.R., et al. Physical Review Letters **97** (2006) 165002.
[22]. BONCAGNI, L., et al. Fusion Engineering and Design (2013), http://dx.doi.org/10.1016/j.fusengdes.2013.02.170
[23]. GILL, R.D., Nuclear Fusion **33** (1993) 1613.

[24]. JAMES, A.N., HOLLMANN, E.M., and TYNAN, G.R., Review of Scientific Instruments **81** (2010) 10E306.
[25]. ESPOSITO, B., et al. Physics of Plasmas **10** (2003) 2350.
[26]. BERTALOT, L., et al. Review of Scientific Instruments **63** (1992) 4554
[27]. YOSHINO, R., and TOKUDA, S., Nuclear Fusion **40** (2000) 1293.
[28]. HELANDER, P., Physics of Plasmas **14** (2007) 122102.
[29]. FORSTER, M., et al., Physics of Plasmas **19** (2012) 052506.
[30]. ARNOUX, G., et al., Journal of Nuclear Materials **415** (2011) 5187.
[31]. BOZHENKOV, S.A., et al., Plasma Physics and Controlled Fusion **50** (2008) 105007.
[32]. YAMAZAKI, K. and SCHMIDT, G.L., Nuclear Fusion **24** (1984) 467.
[33]. RICCARDO, V., et al. Plasma Physics and Controlled Fusion **44** (2002) 905.
[34]. CONNOR, J.W. and HASTIE, R.J., Nuclear Fusion **15** (1975) 415.
[35]. HOLLMANN, E., et al., in Fusion Energy 2012 (Proc. 24th Int. Conf., San Diego, 2012) (Vienna: IAEA) CD-ROM file EX/9-2; accepted for publication in Nuclear Fusion.
[36]. PLYUSNIN, V.V., et al., in Fusion Energy 2012 (Proc. 24th Int. Conf., San Diego, 2012) (Vienna: IAEA) CD-ROM file EX/P8-05.
[37]. RICCARDO, V., et al., Plasma Physics and Controlled Fusion **52** (2010) 124018.
[38]. CARSLAW, H.S., JAEGER, J.C., Conduction of Heat in Solids, Oxford Universty Press, London, 1959.
[39]. VanSANT, J.H., Conduction Heat Transfer Solutions, UCRL-52863, Lawrence Livermore National Lab., 1980.
[40]. MADDALUNO, G., et al., Journal of Nuclear Materials **313-316** (2003) 651.
[41]. BAZYLEV, B., et al., Journal of Nuclear Materials **415** (2011) S841.
[42]. BAZYLEV, B., et al., Journal of Nuclear Materials **438** (2013) S237.
[43]. PUTVINSKI, S., et al., in Fusion Energy 2010 (Proc. 23rd Int. Conf., Daejeon, 2010) (Vienna: IAEA) CD-ROM file ITR/1-6.
[44]. EIDIETIS, N.W. et al., Physics of Plasmas **19** (2012) 056109.
[45]. LUKASH, V.E., et al., "Study of ITER plasma position control during disruptions with formation of runaway electrons", 40th EPS Conf. on Plasma Physics (Helsinki, Finland, 2013) P-5.167.

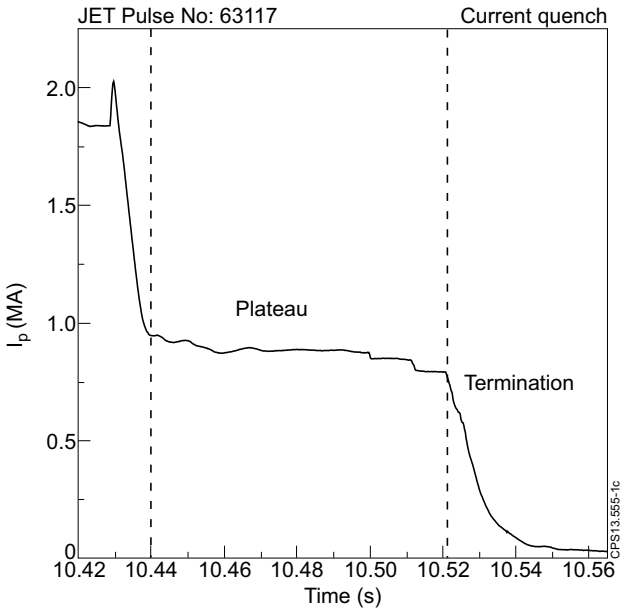


*Figure 1: Time evolution of the plasma current, $I_p$, during a JET disruption showing the current quench, plateau and current termination phases.*

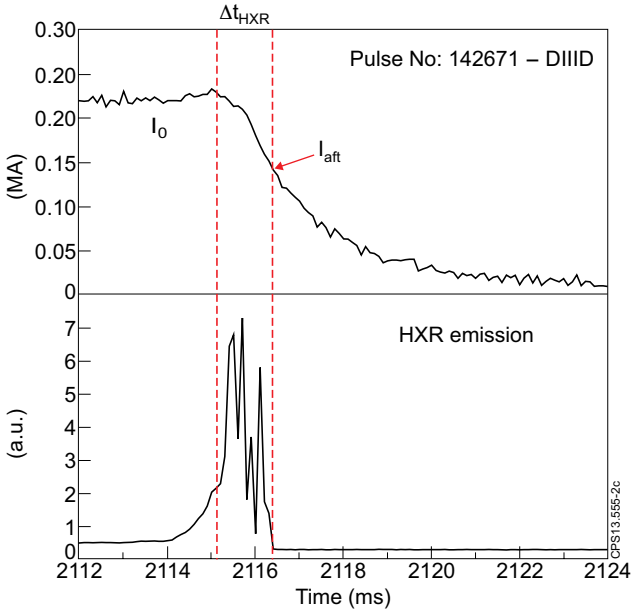


*Figure 2: Plasma current (top) and HXR emission (bottom) time evolution during the termination phase of a DIII-D disruption. I0 is the plateau runaway current following the current quench phase of the disruption and Iaft the residual resistive current after the runaway loss time interval, $\Delta t_{hxr/neut}$, $I_{aft} \equiv I_p\,(t = \Delta t_{hxr/neut})$.*

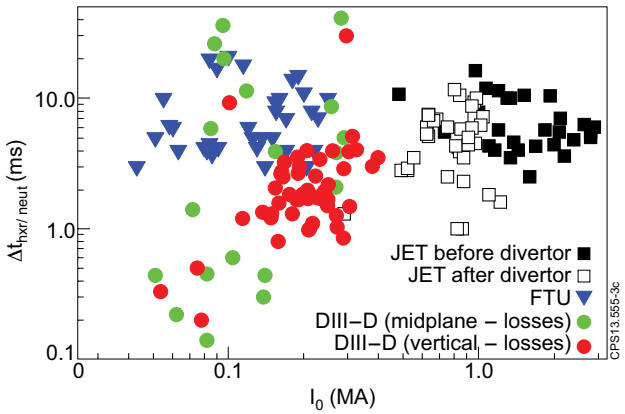


*Figure 3: Runaway loss time interval, $\Delta t_{hxr/neut}$, versus plateau runaway current, $I_0$, for JET, DIII-D and FTU disruption current terminations.*

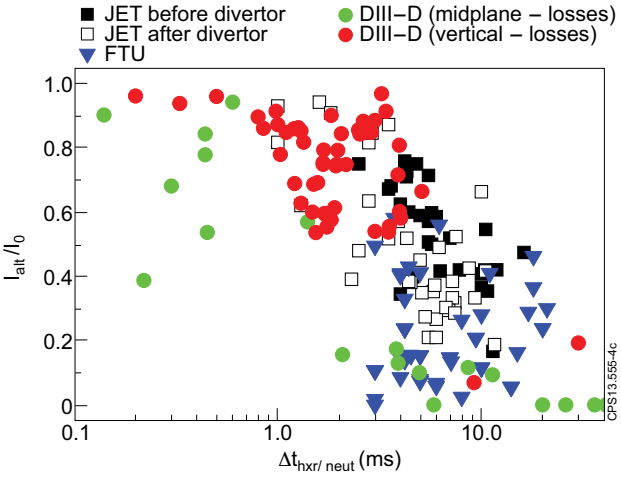


*Figure 4: Ratio of the post-runaway plasma current to the runaway plateau plasma current, $I_{aft}/I_0$, versus the measured time interval for runaway electron loss, $\Delta t_{hxr}/_{neut}$, for the three devices (JET, DIII-D and FTU).*

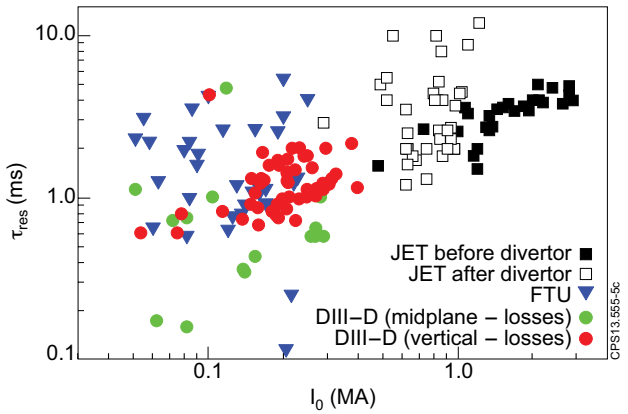


*Figure 5: Resistive time of the residual plasma after runaway loss, $\tau_{res}$, versus plateau runaway current, $I_0$, for the three analyzed devices.*

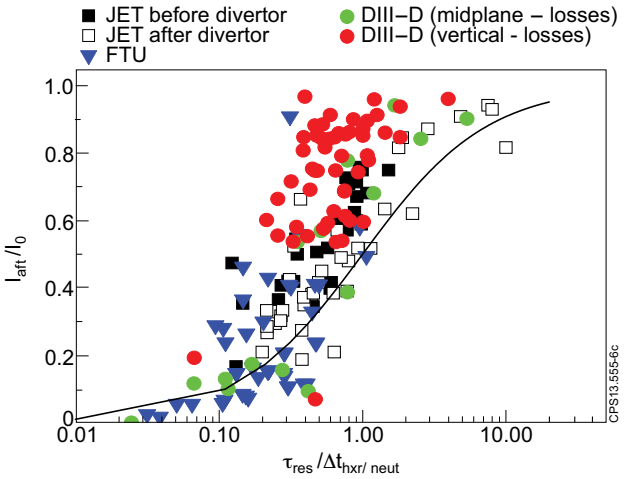


*Figure 6: $I_{aft}/I_0$ versus res=$\Delta t_{hxr/neut}$ for the termination of runaway plateau plasmas in JET, DIII-D and FTU. The full line indicates the phenomenological relation (4) for $I_{aft}/I_0$.*

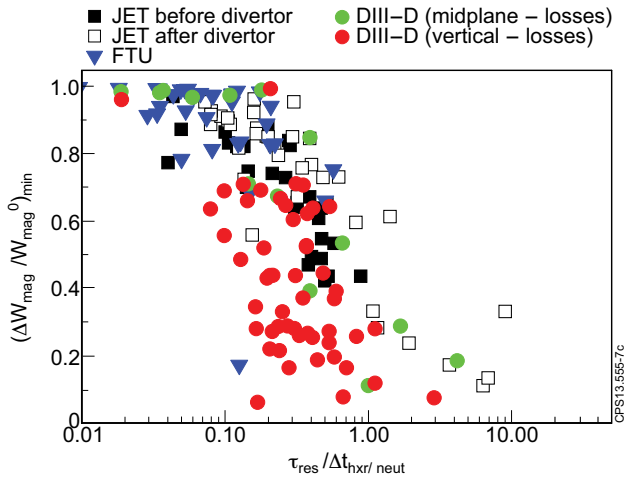


*Figure 7: Minimum fraction of plateau magnetic energy lost during the runaway loss period, $\Delta W_{mag}/W^0_{mag}$, versus $\tau_{res}=\Delta t_{hxr/neut}$ for the analyzed disruption termination phases.*

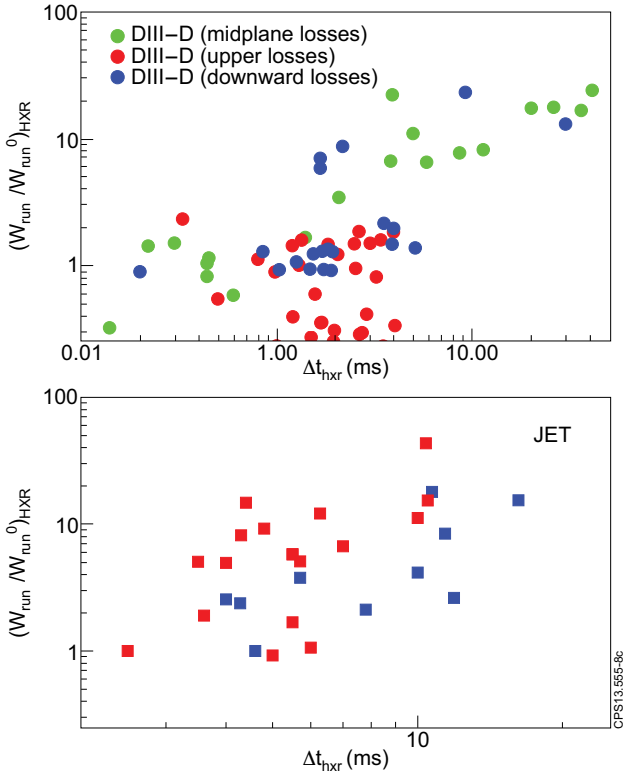


*Figure 8: Top: Estimates, based on HXR measurements, of the runaway kinetic energy increase, ($W_{run}=W^0_{run}$) HXR ($W_{run}$: total runaway kinetic energy; $W^0_{run}$: runaway kinetic energy of the plateau runaway beam, before the loss phase), versus $\Delta t_{hxr}$ during the termination phase of DIII-D disruptions; Bottom: Estimated ($W_{run}/W^0_{run}$)HXR during the termination phase of JET disruptions before the MK-IIA divertor installation. The different colours correspond to different experimental campaigns (filled-blue point with discrete limiters and filled-red points with belt limiters), as the HRX signal in JET is not absolutely calibrated.*

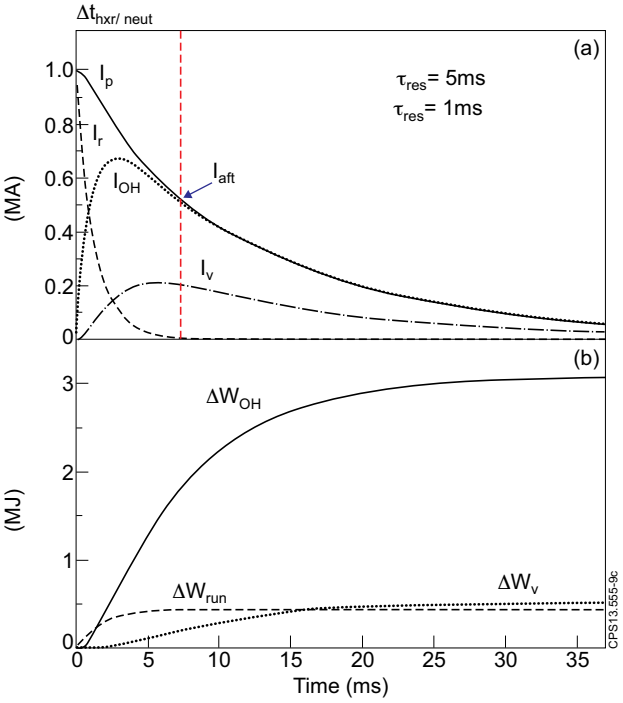


*Figure 9: Simulation of the termination of a 1MA JET runaway plateau: (a) Calculated time evolution of the plasma current, $I_p$, ohmic current, $I_{OH}$, runaway current, $I_r$, and vessel current, $I_v$; (b) Time evolution of the energy ohmically dissipated by the thermal plasma, WOH, converted into runaway kinetic energy, $W_{run}$, and resistively dissipated in the vessel ($\tau_{res}$ = 5ms; $\tau_{diff}$ = 1ms).*

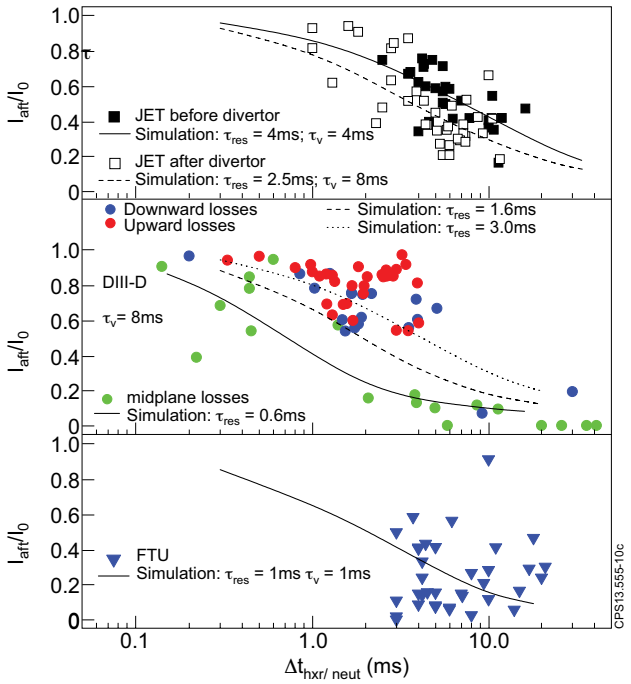


*Figure 10: Comparison between the measured $I_{aft}/I_0$, as a function of $\Delta t_{hxr/neut}$, and the simulations for the termination of runaway plateau plasmas in JET, DIII-D and FTU.*

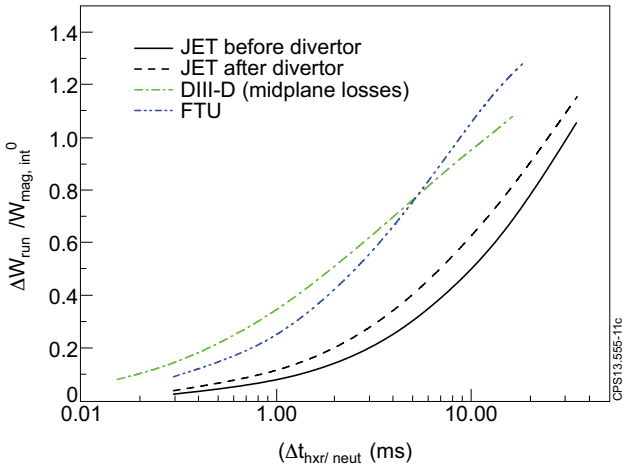


*Figure 11: Ratio of the calculated runaway kinetic energy gain to the plateau internal magnetic energy during current termination versus time interval for runaway loss, $\Delta t_{hxr/neut}$, for the simulations of Fig.10.*

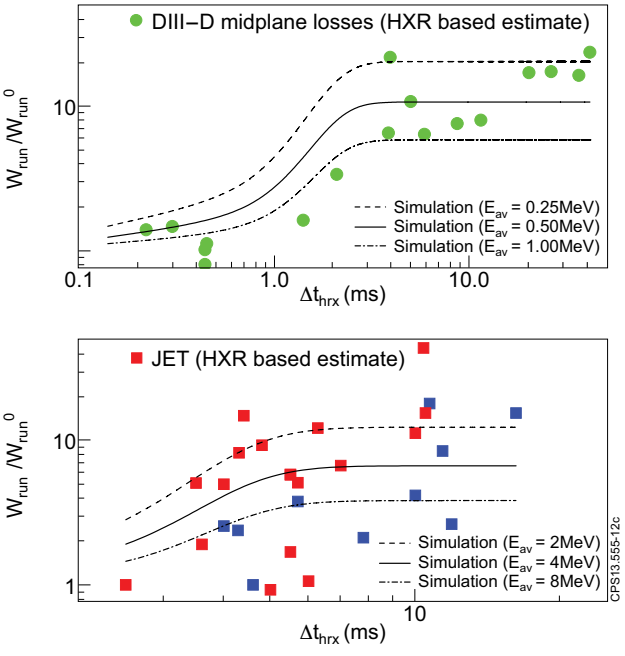


*Figure 12: Comparison between the estimates of $W_{run}/W_0$ run based on the model equations and those based on HXR emission measurements in DIII-D and JET before divertor installation (Fig.8).*

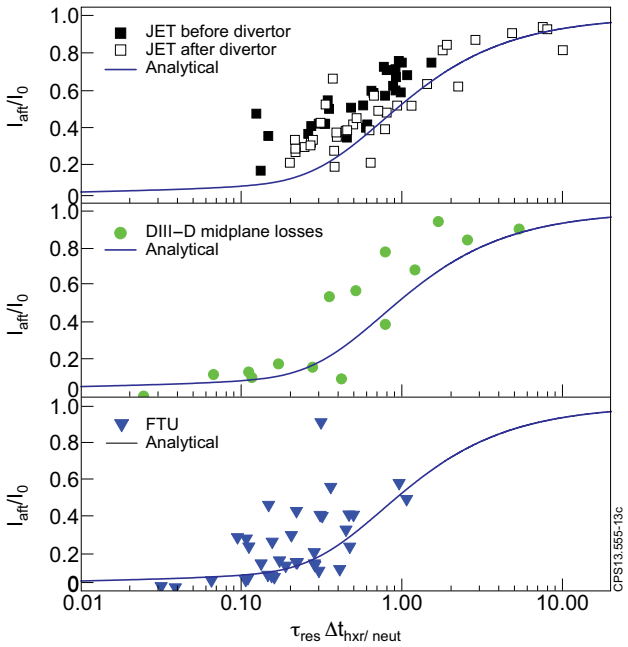


*Figure 13: Comparison between the measured $I_{aft}/I_0$ versus $\tau_{res}/\Delta t_{hxr/neut}$ and the analytical approximation [Eq. (23)] for JET, DIII-D (midplane losses) and FTU current terminations.*

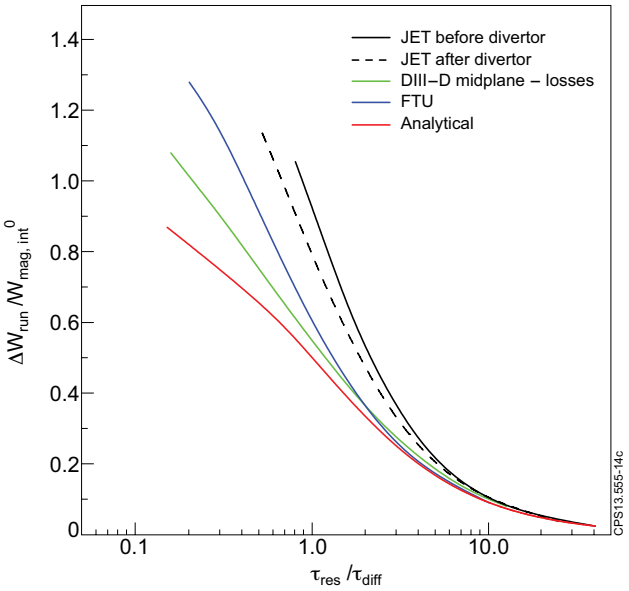


*Figure 14: Calculated $\Delta W_{run}/W^0_{mag;int}$ versus $\tau_{res}/\tau_{diff}$ for the analytical zero order model [Eq. (25)] (red line) and full model numerical simulations for JET, DIII-D and FTU terminations.*

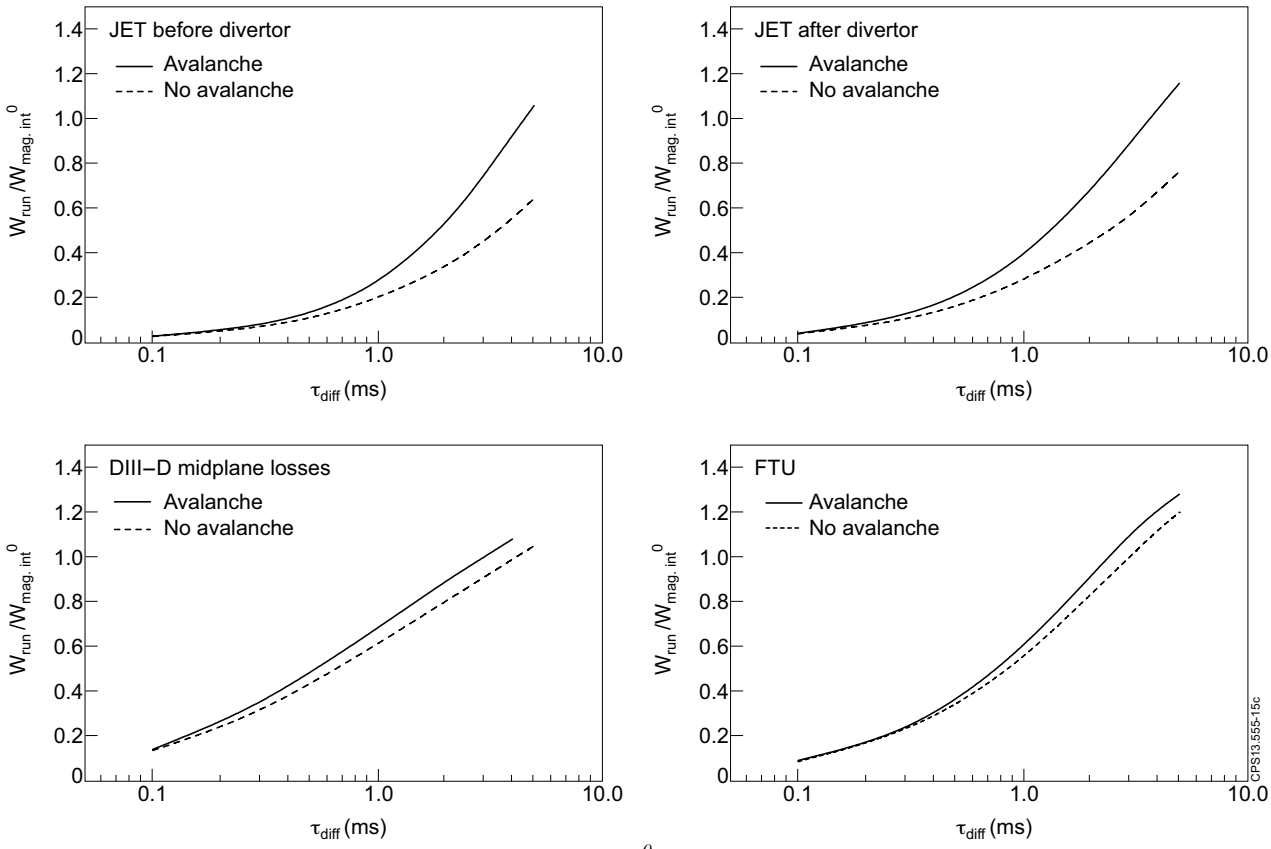


*Figure 15: Comparison between the predicted $\Delta W_{run}/W^0_{mag;int}$ versus $\tau_{diff}$ with (full line) and without (dashed line)including runaway avalanche generation for the same JET, DIII-D and FTU parameters as Fig.11.*

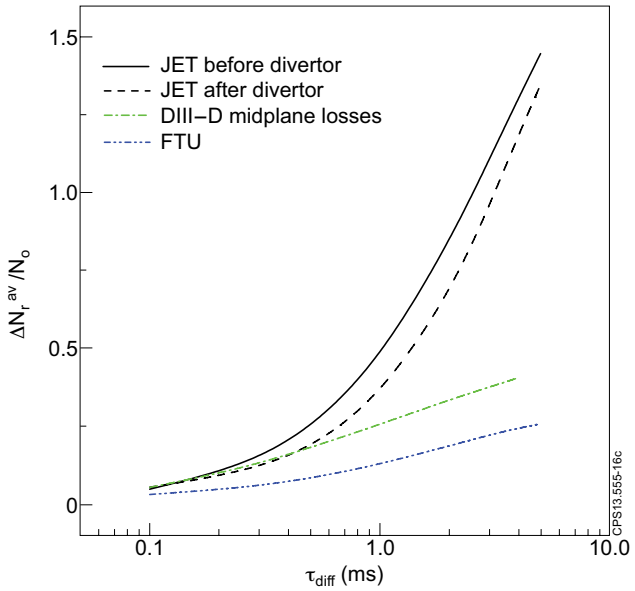


*Figure 16: Estimated avalanche runaway population growth (normalized to the plateau runaway population), $\Delta N_r^{av}/N_0$, versus $\tau_{diff}$ for the same runaway terminations as in Fig.15.*

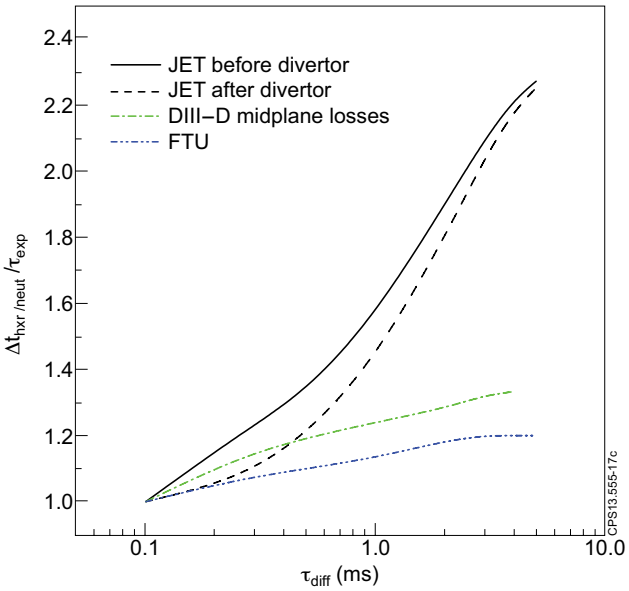


*Figure 17: $\Delta t_{hxr/neut}/\tau_{exp}$ versus $\tau_{diff}$ for the simulation of runaway terminations in JET, DIII-D and FTU.*

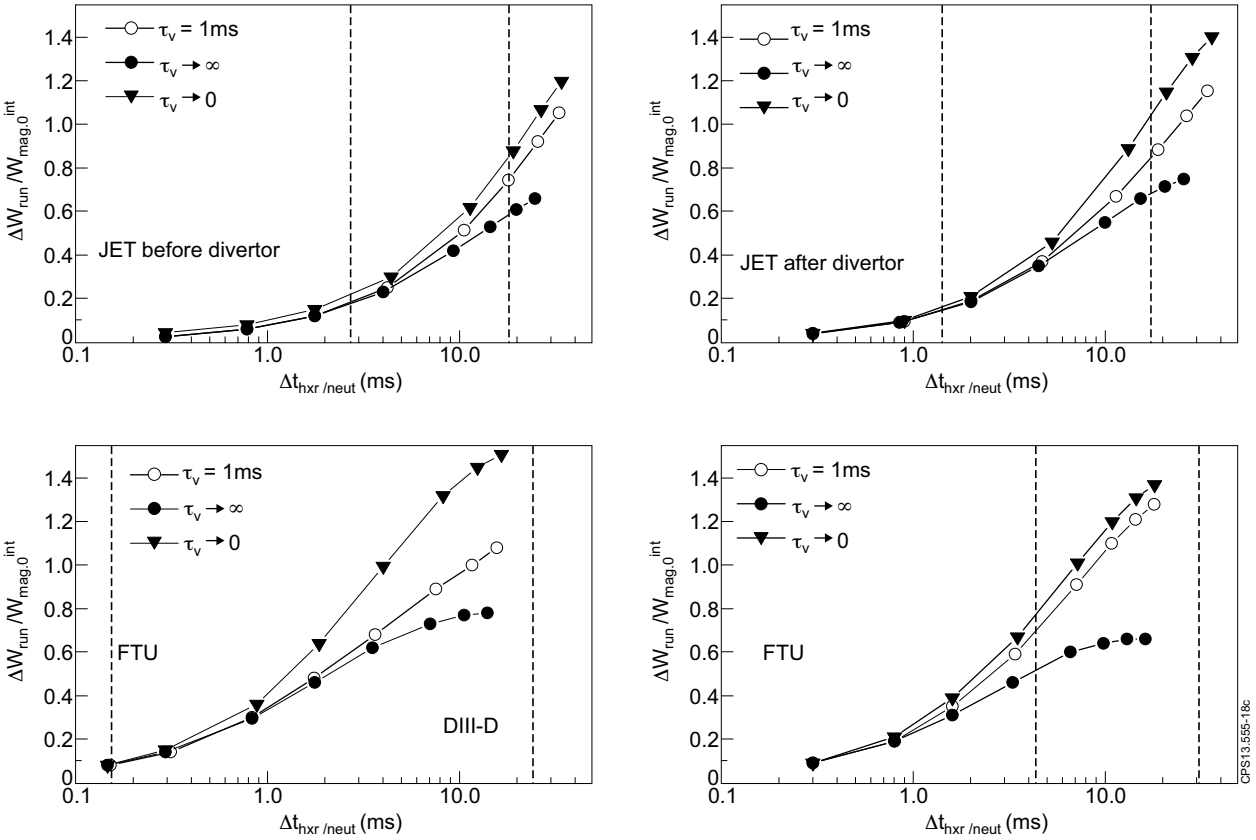


*Figure 18: Calculated $\Delta W_{run}/W^0_{mag;int}$ versus $\Delta t_{hxr/neut}$ for JET (before and after divertor installation), DIII-D and FTU terminations: Open circles: numerical simulations in Fig.11; Black circles: perfectly conducting vacuum vessel limit ($\tau_v \to \infty$); Black triangles: infinitely resistive vacuum vessel limit ($\tau_v \to 0$).*

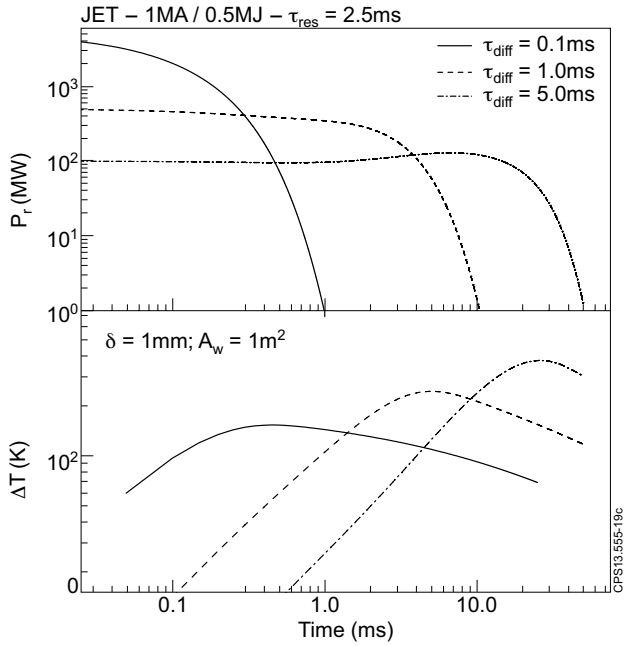


*Figure 19: Typical 1MA JET runaway plateau current termination after divertor installation: Top: Time evolution of the power loads due to the runaway electrons, $P_r(t)$ (energy deposited by the runaways/time); Bottom: Surface temperature rise due the runaway heat loads for JET CFC plasma facing components for 1mm runaway electron deposition depth and $A_w = 1m^2$. The plateau runaway kinetic energy is $W^0_{run} = 0.5MJ$ and $\tau_{diff} = 0.1, 1,$ and 5ms.*

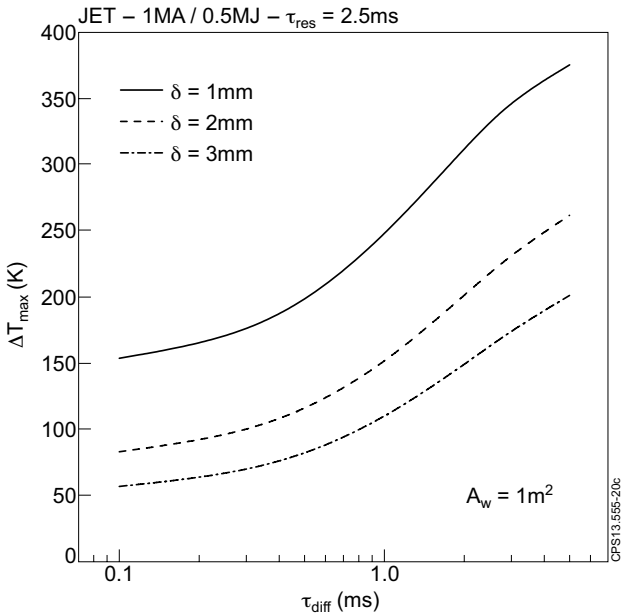


*Figure 20: Maximum $\Delta T$ in the JET CFC first wall plasma facing components as a function of $\tau_{diff}$ for $I_0 = 1MA$, $W^0_{run} = 0.5MJ$ and $\delta = 1, 2, 3mm$.*

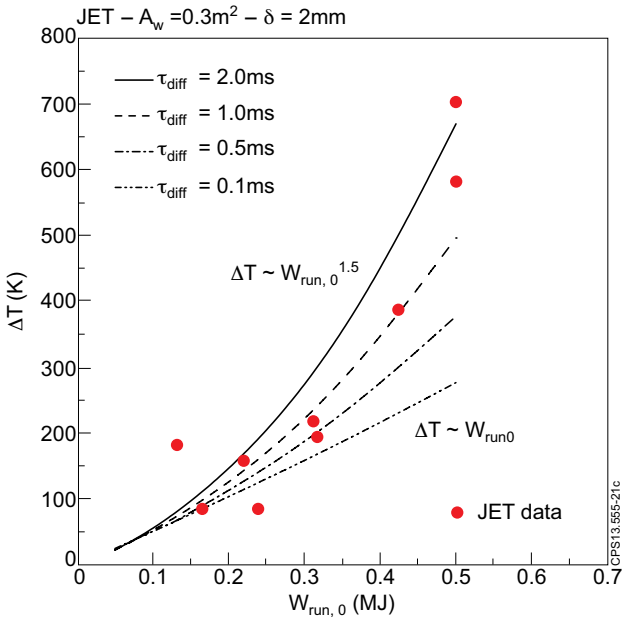


*Figure 21: Estimated surface temperature rise in JET CFC upper dump plate versus plateau runaway beam energy for $\tau_{diff} = 0.1, 0.5, 1$ and 2ms. The energy is assumed proportional to $I_0$ (0.5MJ for 1MA), $\delta = 2mm$ and $A_w = 0.3m^2$. The temperature increase due to runaway electrons measured in a set JET disruptions triggered by MGI [37] is also included for comparison (red dots).*

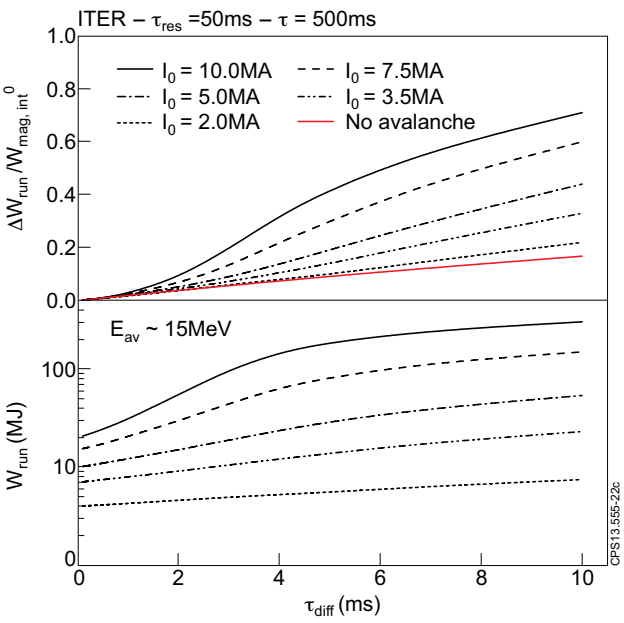


*Figure 22: Top: $\Delta W_{run}/W^0_{mag;int}$ versus $\tau_{diff}$ for ITER current terminations ($I_0 = 2, 3.5, 5, 7.5$ and 10MA). For comparison, the red line shows the predictions assuming no avalanche generation of runaways during termination; Bottom: For the same plateau runaway currents, total energy deposited by the runaway electrons, $W_{run} / W^0_{run} + \Delta W_{run}$, versus $\tau_{diff}$.*

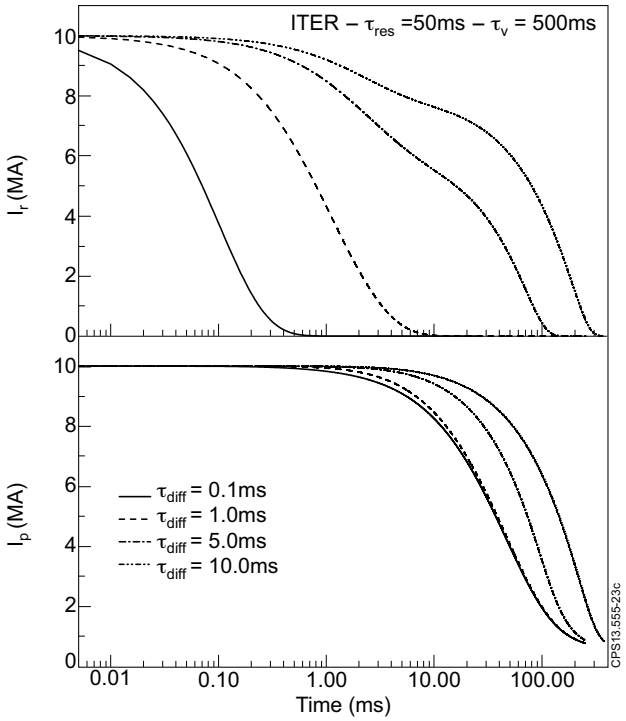


*Figure 23: Time evolution of the runaway current (top) and of the total plasma current (bottom) during the termination phase of a 10MA ITER plateau current ($\tau_{diff}$ = 0.1,1, 3 and 10ms).*

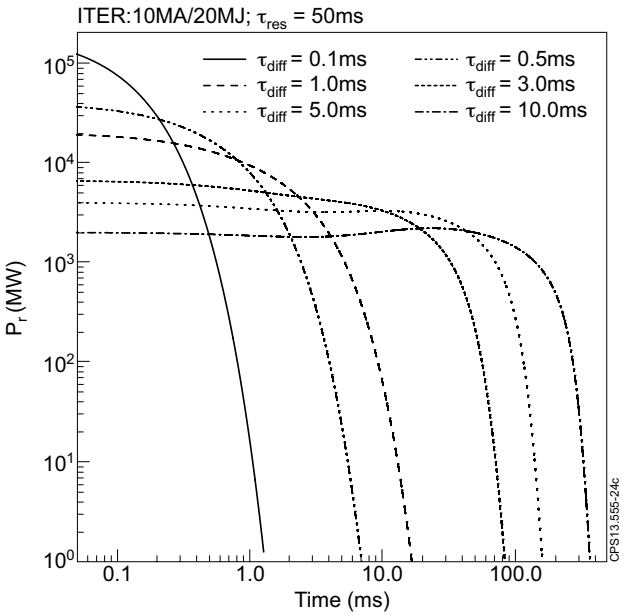


*Figure 24: Time evolution of the power loads due to the runaway electrons during termination of a 10MA runaway plateau plasma in ITER ($\tau_{diff}$ = 0.1, 0.25, 0.5, 1, 3, 5 and 10ms). The initial plateau runaway kinetic energy is $W^0_{run}$ = 20MJ.*

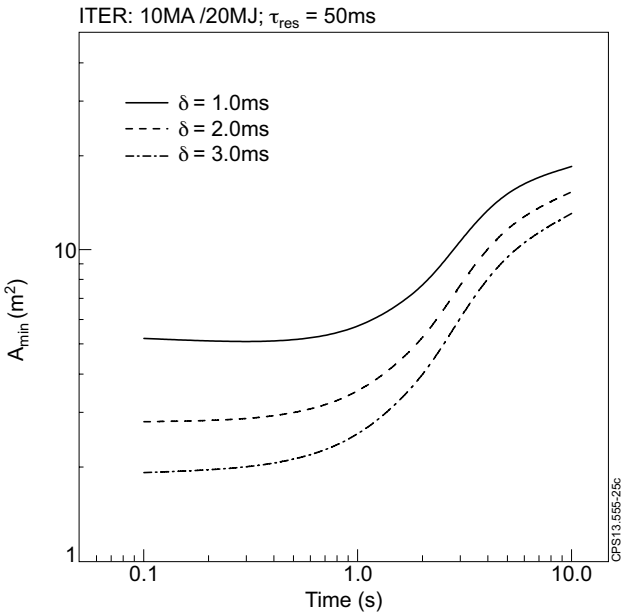


*Figure 25: Minimum wetted area to avoid Be melting in ITER as a function of diff for $I_0$ = 10 MA; $W^0_{run}$ = 20MJ and = 1; 2; 3mm ($\tau_{res}$ = 50ms; v = 500ms).*

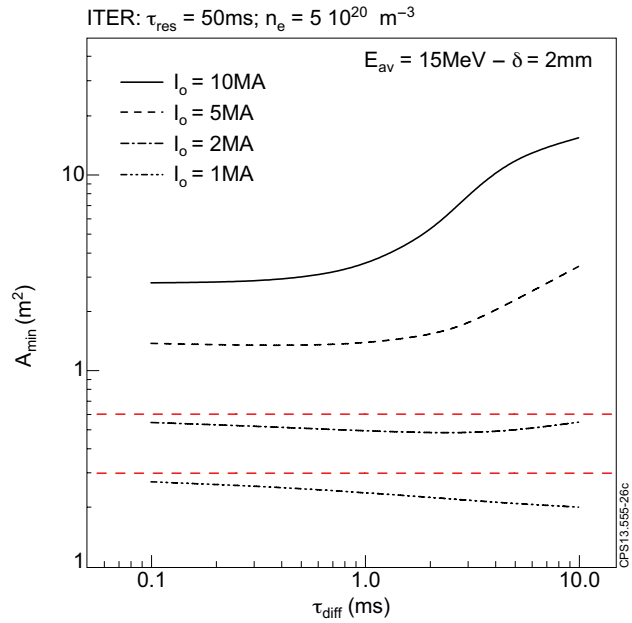


*Figure 26: ITER Amin versus $\tau_{diff}$ for $I_0$ = 1, 2, 5 and 10MA, $E_{av}$ = 15MeV and = 2mm ($\tau_{res}$ = 50ms; v = 500ms; $n_e$ = $5\times10^{20}$ $m^{-3}$). The horizontal red dashed lines indicate the estimated runaway wetted area in ITER, ~ 0.3 – 0.6$m^2$.*

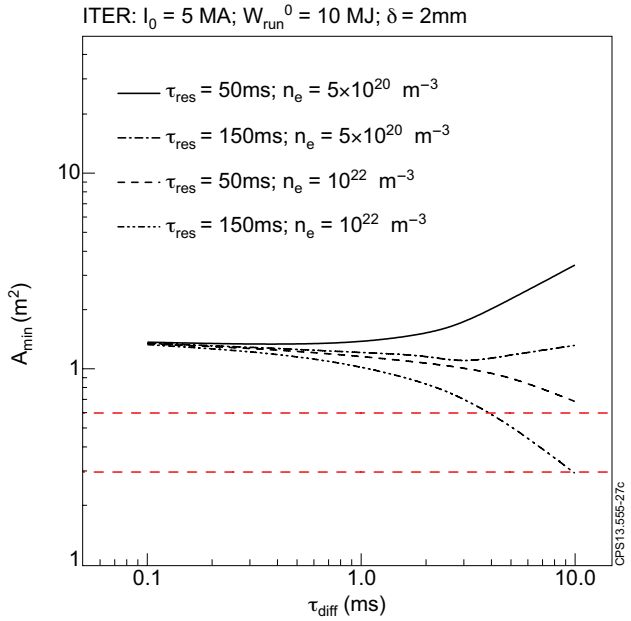


*Figure 27: $A_{min}$ versus $\tau_{diff}$ for a 5MA ITER termination, $W^0_{run}$ = 10MJ (Eav ~ 15MeV), δ = 2mm, $\tau_{res}$ = 50, 150ms and ne = 5×10^20; 10^22 m^−3. The horizontal dashed lines lines correspond to the estimates for the runaway wetted area in ITER, ~ 0.3–0.6m^2.*

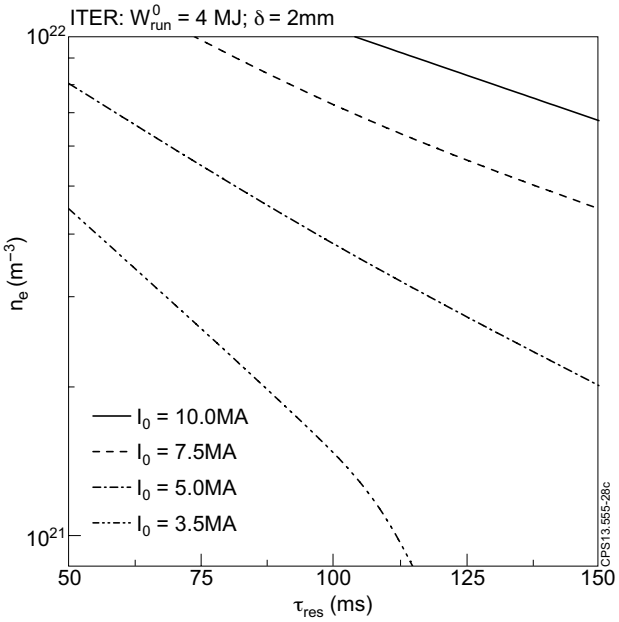


*Figure 28: Minimum plasma density required to keep $A_{min}$ below ~ 0.6m^2 versus res during the the termination phase of ITER disruptions ($I_0$ = 3.5, 5, 7.5, 10MA), assuming δ= 2mm and $W^0_{run}$ = 4 MJ.*